2013-12

Performance improvements to the Naval Postgraduate School Turbopropulsion Labs Transonic Axially Splittered Rrotor

Lehrfeld, Michael C.

Monterey, California: Naval Postgraduate School

NAVAL POSTGRADUATE SCHOOL

MONTEREY, CALIFORNIA

THESIS

PERFORMANCE IMPROVEMENTS TO THE NAVAL POSTGRADUATE SCHOOL TURBOPROPULSION LABS TRANSONIC AXIALLY SPLITTERED ROTOR

by

Michael C. Lehrfeld

December 2013

Thesis Co-Advisors: Anthony J. Gannon
Garth V. Hobson

THIS PAGE INTENTIONALLY LEFT BLANK

REPORT DOCUMENTATION PAGE			Form Approved OMB No. 0704-0188
Public reporting burden for this collection of information is estimated to average 1 hour per response, including the time for reviewing instruction, searching existing data sources, gathering and maintaining the data needed, and completing and reviewing the collection of information. Send comments regarding this burden estimate or any other aspect of this collection of information, including suggestions for reducing this burden, to Washington headquarters Services, Directorate for Information Operations and Reports, 1215 Jefferson Davis Highway, Suite 1204, Arlington, VA 22202-4302, and to the Office of Management and Budget, Paperwork Reduction Project (0704-0188) Washington DC 20503.			
1. AGENCY USE ONLY *(Leave blank)*	**2. REPORT DATE** December 2013	**3. REPORT TYPE AND DATES COVERED** Master's Thesis	
4. TITLE AND SUBTITLE PERFORMANCE IMPROVEMENTS TO THE NAVAL POSTGRADUATE SCHOOL TURBOPROPULSION LABS TRANSONIC AXIALLY SPLITTERED ROTOR		**5. FUNDING NUMBERS**	
6. AUTHOR(S) Michael C. Lehrfeld			
7. PERFORMING ORGANIZATION NAME(S) AND ADDRESS(ES) Naval Postgraduate School Monterey, CA 93943-5000		**8. PERFORMING ORGANIZATION REPORT NUMBER**	
9. SPONSORING /MONITORING AGENCY NAME(S) AND ADDRESS(ES) U.S. Army Research Laboratory, Mechanical Sciences Division, Research Triangle Park, NC 27709-2211		**10. SPONSORING/MONITORING AGENCY REPORT NUMBER**	
11. SUPPLEMENTARY NOTES The views expressed in this thesis are those of the author and do not reflect the official policy or position of the Department of Defense or the U.S. Government. IRB protocol number ____N/A____.			
12a. DISTRIBUTION / AVAILABILITY STATEMENT Approved for public release; distribution is unlimited		**12b. DISTRIBUTION CODE** A	

13. ABSTRACT (maximum 200 words)

Performance improvement investigations to the Naval Postgraduate School Turbo Propulsion Laboratory's (NPS TPL) Transonic Axially Splittered Rotor were investigated. Implementation of current NPS TPL design procedure that uses COTS software (MATLAB, SolidWorks, and ANSYS-CFX) for the geometric rendering and analysis was modified and documented. Numerical simulations were conducted and experimental data were collected at the NPS TPL utilizing the transonic compressor rig. This study advanced the understanding of casing tip gap, rotor-stator interaction, stator relative blade placement of a hybrid tandem/splittered design, and performance benefits.

The reduction in rotor tip gap produced higher performance bench marks as predicted. The addition and analysis of multiple blade rows proved to be straight forward and the design methodology and in house procedure was further optimized. While other studies sought to affect the pressure surface of the lead blade, it was determined that using the trailing blade to influence the high momentum flow over suction surface of the lead blade produced better performance gains With tip gap closure and the addition of the stator stage, rotor alone performance was improved from experimentally measured peak total-to-total pressure ratio of 1.69 to 1.99 and the peak total-to-total isentropic efficiency from 72 to 77 percent at 100 percent design speed.

14. SUBJECT TERMS Turbomachinery, axial compressor, splittered rotor, hybrid stator			**15. NUMBER OF PAGES** 71
			16. PRICE CODE
17. SECURITY CLASSIFICATION OF REPORT Unclassified	**18. SECURITY CLASSIFICATION OF THIS PAGE** Unclassified	**19. SECURITY CLASSIFICATION OF ABSTRACT** Unclassified	**20. LIMITATION OF ABSTRACT** UU

NSN 7540-01-280-5500 Standard Form 298 (Rev. 2-89)
Prescribed by ANSI Std. 239-18

THIS PAGE INTENTIONALLY LEFT BLANK

Approved for public release; distribution is unlimited

PERFORMANCE IMPROVEMENTS TO THE NAVAL POSTGRADUATE SCHOOL TURBOPROPULSION LABS TRANSONIC AXIALLY SPLITTERED ROTOR

Michael C. Lehrfeld
Lieutenant Commander, United States Navy
B.S., University of Maryland, 1997

Submitted in partial fulfillment of the
requirements for the degree of

MASTER OF SCIENCE IN ASTRONAUTICAL ENGINEERING

from the

NAVAL POSTGRADUATE SCHOOL
December 2013

Author: Michael C. Lehrfeld

Approved by: Anthony J. Gannon
Thesis Co-Advisor

Garth V. Hobson
Thesis Co-Advisor,

Knox T. Millsaps
Chair, Department of Mechanical and Aerospace Engineering

THIS PAGE INTENTIONALLY LEFT BLANK

ABSTRACT

Performance improvement investigations to the Naval Postgraduate School Turbo Propulsion Laboratory's (NPS TPL) Transonic Axially Splittered Rotor were investigated. Implementation of current NPS TPL design procedure that uses commercial-off-the-shelf software (MATLAB, SolidWorks, and ANSYS-CFX) for the geometric rendering and analysis was modified and documented. Numerical simulations were conducted and experimental data were collected at the NPS TPL utilizing the transonic compressor rig. This study advanced the understanding of blade-casing tip gap, rotor-stator interaction, stator relative blade placement of a hybrid tandem/splittered design, and performance benefits.

The reduction in rotor tip gap produced higher performance bench marks as predicted. The addition and analysis of multiple blade rows proved to be straight forward and the design methodology and in house procedure was further optimized. While other studies sought to affect the pressure surface of the lead blade, it was determined that using the trailing blade to influence the high momentum flow over suction surface of the lead blade produced better performance gains With tip gap closure and the addition of the stator stage, rotor alone performance was improved from experimentally measured peak total-to-total pressure ratio of 1.69 to 1.99 and the peak total-to-total isentropic efficiency from 72 to 77 percent at 100 percent design speed.

THIS PAGE INTENTIONALLY LEFT BLANK

TABLE OF CONTENTS

THIS PAGE INTENTIONALLY LEFT BLANK

LIST OF FIGURES

THIS PAGE INTENTIONALLY LEFT BLANK

LIST OF TABLES

THIS PAGE INTENTIONALLY LEFT BLANK

LIST OF ACRONYMS AND ABBREVIATIONS

CFD	computational fluid dynamics
CFX	The CFD simulation program in ANSYS Workbench.
CFX-Pre	CFX boundary conditions and solver settings module.
CFX-Solver	CFX solver program.
CFX-Post	CFX post processing
LE	leading edge (blade)
MB	main blade
NPS	Naval Postgraduate School
PS	pressure side
SB	splitter blade
SS	suction side
SolidWorks	a solid modeling program
TASR	TPL Axial Splittered Rotor
TE	trailing edge (blade)
TG	tip gap
TCR	Transonic Compressor Rig
TPL	Turbopropulsion Lab
LB	lead blade (stator)
TB	trail blade (stator)
THS	TPL hybrid stator

THIS PAGE INTENTIONALLY LEFT BLANK

ACKNOWLEDGMENTS

Thank you to my advisors Drs Anthony Gannon and Garth Hobson and CDR Scott Drayton. Without your insight and guidance I'd be floundering at the keyboard. Thank you to John Gibson for allowing me to work in your lab.

Above all, thank you Dawn, for all your understanding and support. Without you nothing is worth it.

THIS PAGE INTENTIONALLY LEFT BLANK

I. INTRODUCTION

A. MOTIVATION

Recent studies at the Naval Postgraduate School (NPS) Turbopropulsion Laboratory (TPL) have explored the design and performance of axial compressors with splitter blades. Historical studies have shown high efficiencies and pressure ratios but with limited mass flow operating ranges. Drayton [1] developed an alternative design geometry and produced and tested the transonic axially splittered rotor (TASR). TASR displayed an isentropic efficiency of 72 percent with a total-to-total pressure ratio of 1.7 when tested with a large tip gap of two percent of blade height.

This study sought to advance the understanding of axial compressor rotors with splitter blades through the experimental investigation of blade to case tip gap (TG) distance and its effect on stage efficiency and pressure ratio. Additionally, Drayton's design tools were modified to produce a simulated stator stage to be paired with the TASR. Smaller form factor engine stages with performance of multiple traditional stages will lead to overall smaller gas turbine engines with no penalty in performance or same form factor with increased performance and less complexity.

B. PREVIOUS WORK

1. Rotor Tip Gap

While the Drayton design was influenced by Wennerstrom [2], [3], Tzuoo [4] and McClumphy [5], the design departed from previous work in the areas of blade geometry, placement, blade number and solidity. At 100 percent speed, Wennerstrom demonstrated total-to-total peaks of 3.47 in pressure ratio and 85 percent in isentropic efficiency. Mass flow rate range was three percent. Figure 1 depicts Wennerstrom's design with 60 blades, with 30 main blades (MB) and 30 splitter blades (SB). The splitter blades were 50 percent chord of the main blade and all blades had their trailing edges aligned axially. Drayton reduced the number of blades from 60 to 24 with a large departure in blade geometry and relative position, Figure 2. Pressure ratio of 1.69 and efficiency of 74 percent were measured with a mass flow rate range of 7.5 percent. While total-to-total

performance numbers are considerably lower than Wennerstrom's design, TASR doubles the mass flow rate range. The rotor was tested with large tip gap (TG) clearances to safeguard its integrity during initial testing.

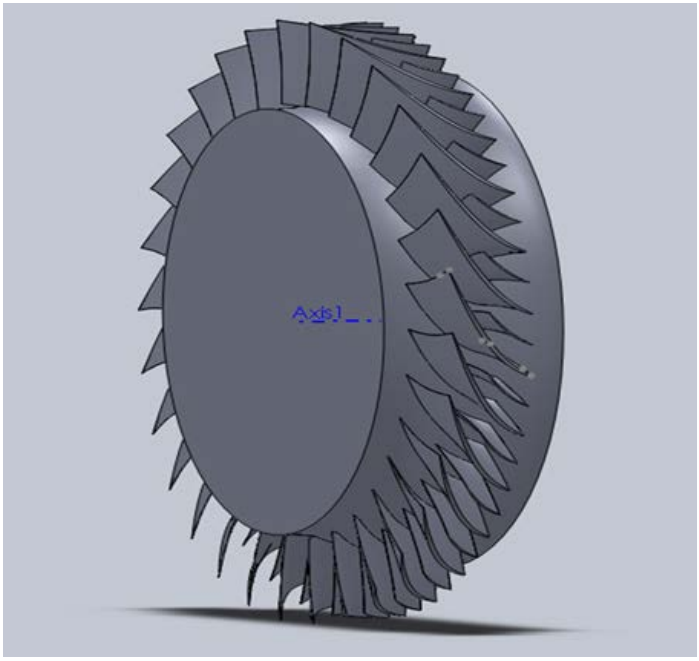

Figure 1. Wennerstrom's transonic axial compressor splittered rotor (after [1])

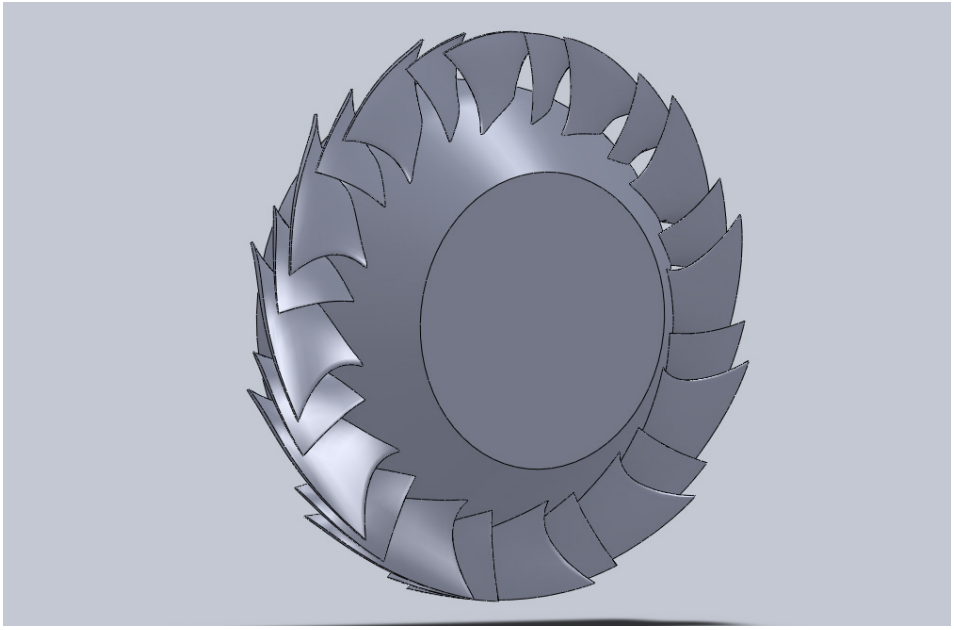

Figure 2. TASR solid model (after [1])

2. Transonic Rotor with Stator Incorporation

No investigations of the NPS TPL rotor paired with a stator design have been conducted. This study is the first to investigate the current NPS rotor geometry with a hybrid splittered/tandem stator design.

C. CURRENT STUDY

Objectives of this study is to modify existing TASR casing to produce smaller TG, test the resultant geometry in comparison to numerical models and previous TG distances. Design, test, and evaluate a tandem stator stage paired with the TASR.

- Further develop NPS TPL design tools for the inclusion of additional blade rows
- Redesign NPS TPL Transonic Compressor Rig (TCR) for a wider range of compressor geometries and improved reliability and survivability
- Decrease rotor-casing tip gap and characterize performance improvements.
- Design a hybrid tandem/splittered stator row to accompany the TPL transonic splittered rotor
- Characterize performance of rotor-stator through numerical methods and incorporate rotor and hybrid stator into TCR

THIS PAGE INTENTIONALLY LEFT BLANK

II. HYBRID STATOR DESIGN

A. TPL DESIGN TOOLS

The TASR, and TPL Hybrid Stator (THS) design was accomplished using the method of Drayton [1] with modifications, for completeness a brief description of the unmodified procedure is contained here. The design goals were to maximize total-to-total isentropic efficiency, maximize total-to-total pressure ratio, and achieve an axial flow field at stage outlet.

A MATLAB 2013a script contained the geometric parameters shown in Appendix A, Table 1. These parameters and other scripts were called to create the rotor hub, spinner, casing and blades. This data was then passed to SolidWorks 2012 to produce a model with the specified geometry. Figures 3-5 show graphical representations of the input parameters as they relate to the physical geometry of blades and the location of the blades on the rotor hub. With the hub, casing and blade boundaries defined, MATLAB instructs SolidWorks to create a fluid domain (or gas path) that fills the space between a main and splitter blade passage. The blades are subtracted from the gas path using a Boolean operation, leaving a representation of a wedge of air containing one set of blades bound by rotor hub and casing. The beginning and end of the wedge is an arbitrary distance from the point of the spinner and the trailing edge of the rotor/stator blade. A representative rotor air wedge beginning upstream of the spinner point and ending at the end of the rotor blisk is shown in Figure 6. The air wedge in parasolid format is then sent to ANSYS-CFX 14.0 where a computational fluid dynamics analysis is performed to produce a compressor performance map. In this study, the rotor air wedge was modified to end at the location shown to accommodate the stator, which is further downstream than Drayton[1], who investigated the rotor only case.

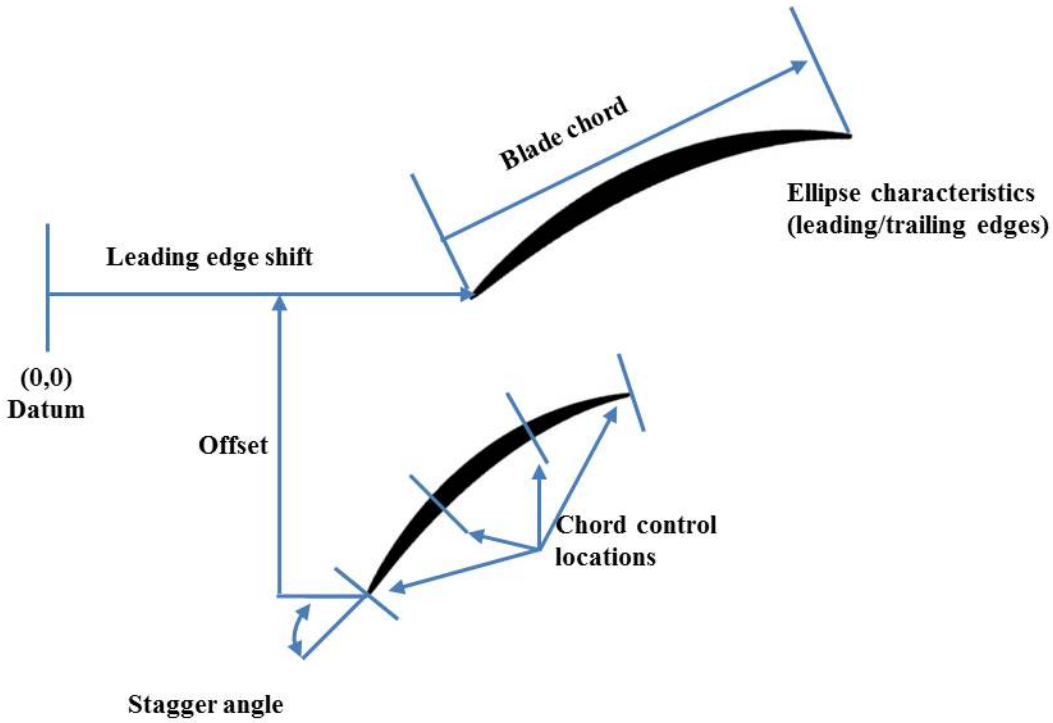

Figure 3. Blade input parameters

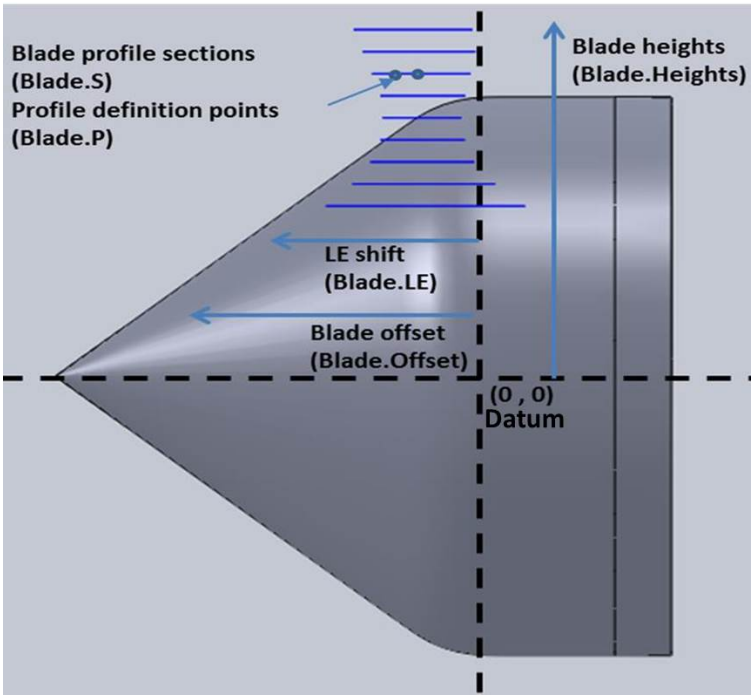

Figure 4. HardCodeBlade passage input parameters (after [1])

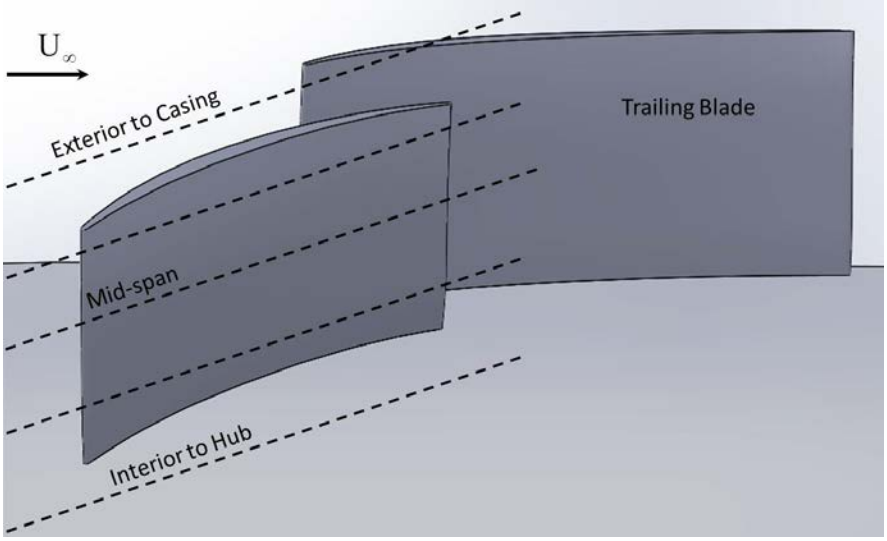

Figure 5. Blade control heights

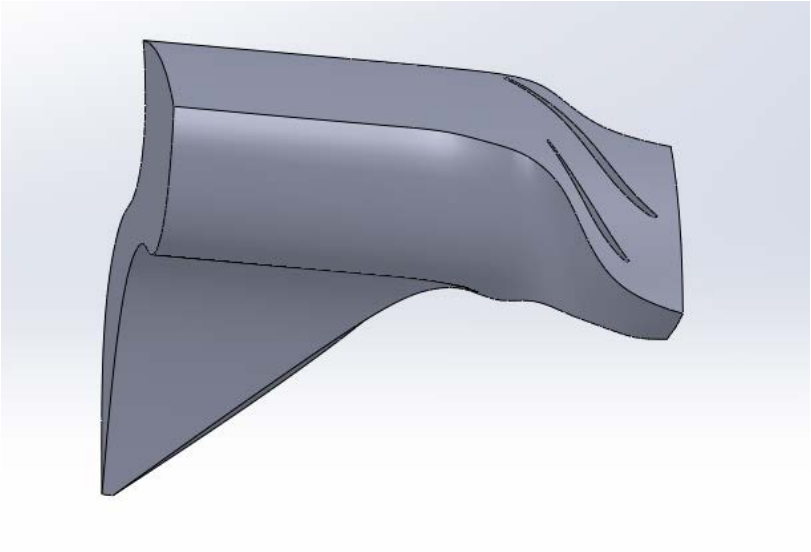

Figure 6. "Single" passage rotor air wedge

B. MODIFICATIONS TO TPL DESIGN TOOL FOR STATOR DESIGN

Using the rotor geometry as a base line design, a blade location parameter was used to move the stator datum 59.69 mm (2.35 inches) further downstream from the zero line shown previously in Figure 4. This placed the leading edges of the stator blades an acceptable distance from the trailing edge of the TASR and allowed for incorporation of additional hub material to structurally support the blades upon manufacture. The rotor air

wedge was initially cut at an arbitrary distance from the trailing edge of the rotor blades. To add the downstream stator blade row, the rotor air wedge had to be cut at the downstream face of the rotor blisk and the upstream portion saved as a SolidWorks part. The THS air wedge is similarly constructed with the portion of the air wedge upstream of the stator blisk discarded. As both air wedges are built on the same coordinate system, combining the two wedges is accomplished by creating an assembly that mates the common surface automatically. Figure 7 shows a completed rotor and stator air wedge. Upstream and downstream air wedge cuts were arbitrary, but attention was paid to having the free stream perpendicular to the inlet face, an adequate upstream distance to from rotor to limit shock smearing, outlet flow that is representative of the resultant vector field after interaction with the stator stage and an undistorted outlet pressure field. Increased computational time associated with larger air wedge volumes was also considered.

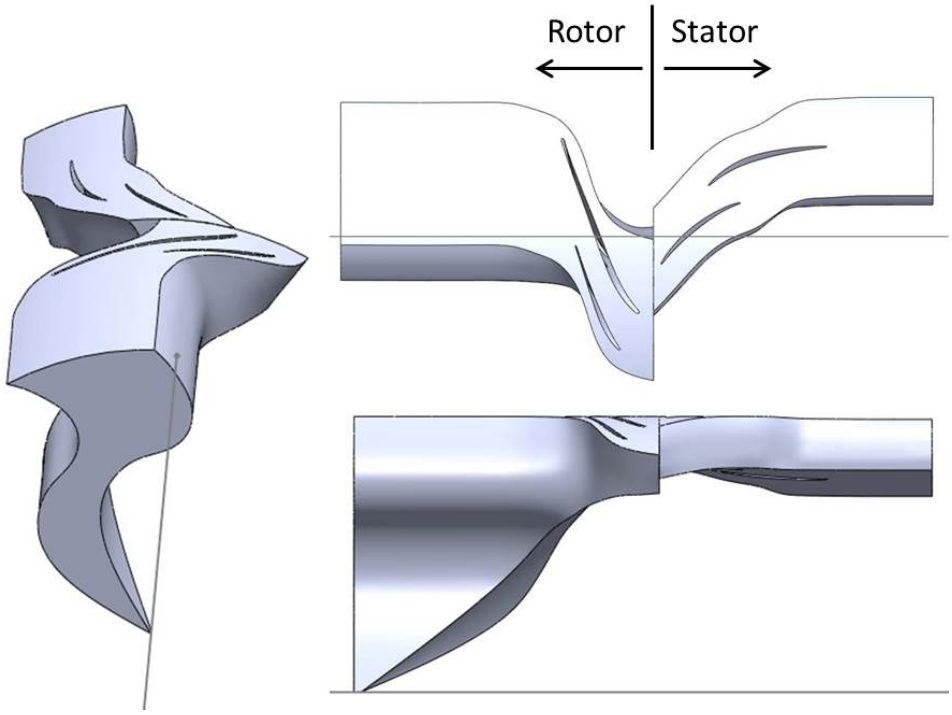

Figure 7. Combined TASR/THS air wedge

The combined air wedge was imported into ANSYS CFX where periodic and interface surfaces were defined. The CFD project was defined as a rotating frame rotor domain and stationary frame stator domain with a stage interface between the two. Fluid parameters, rotational velocity, and outlet back pressure were passed through a MATLAB script interface to ANSYS Workbench. Speed line generation was accomplished through the automation process described in Drayton [1] and through manual individual point investigations.

C. TPL HYBRID STATOR BLADE GEOMETRY DESIGN

The initial blade design involved changing blade parameters from the TASR transonic configuration to shapes more suited to subsonic Mach numbers. The upstream blade on the stator blisk will be referred to as the lead blade (LB) while the tandem/splitter blade will be the trailing blade (TB). Blade chords were 50.8 mm (2 in) and 63.5 mm (2.5 in) for the LB and TB respectively with a trailing edge/leading edge overlap near 12.7 mm (0.5 in).

The geometry design process began with calculating the rotor exit plane average flow angles and manipulating the blade stagger to match LB leading edge angle with the incident flow. Visualization of the vector flow field at various blade heights enabled selection of leading edge stagger angle. LB stagger angles were changed to manipulate blade camber with the goal of turning the flow while minimizing flow separation on the suction side. This evaluation was accomplished through the ANSYS CFX programs resident post processing flow visualization features. Visual inspections of flow field vector plots at five passage heights from hub to casing allowed the tailoring of blade camber to manage flow separation. Representative examples of flow field vector results are show in Figure 8. Once an initial geometry was obtained, the specified backpressure (0.70 to 0.80 atm) was increased to find the point where the mass flow (4.27 to 4.32 kg/s) matched the maximum efficiency points of the rotor at 100 percent operating speed with no tip gap. With this backpressure, THS geometry iterations continued until a maximum isentropic efficiency of 77.5 percent was achieved.

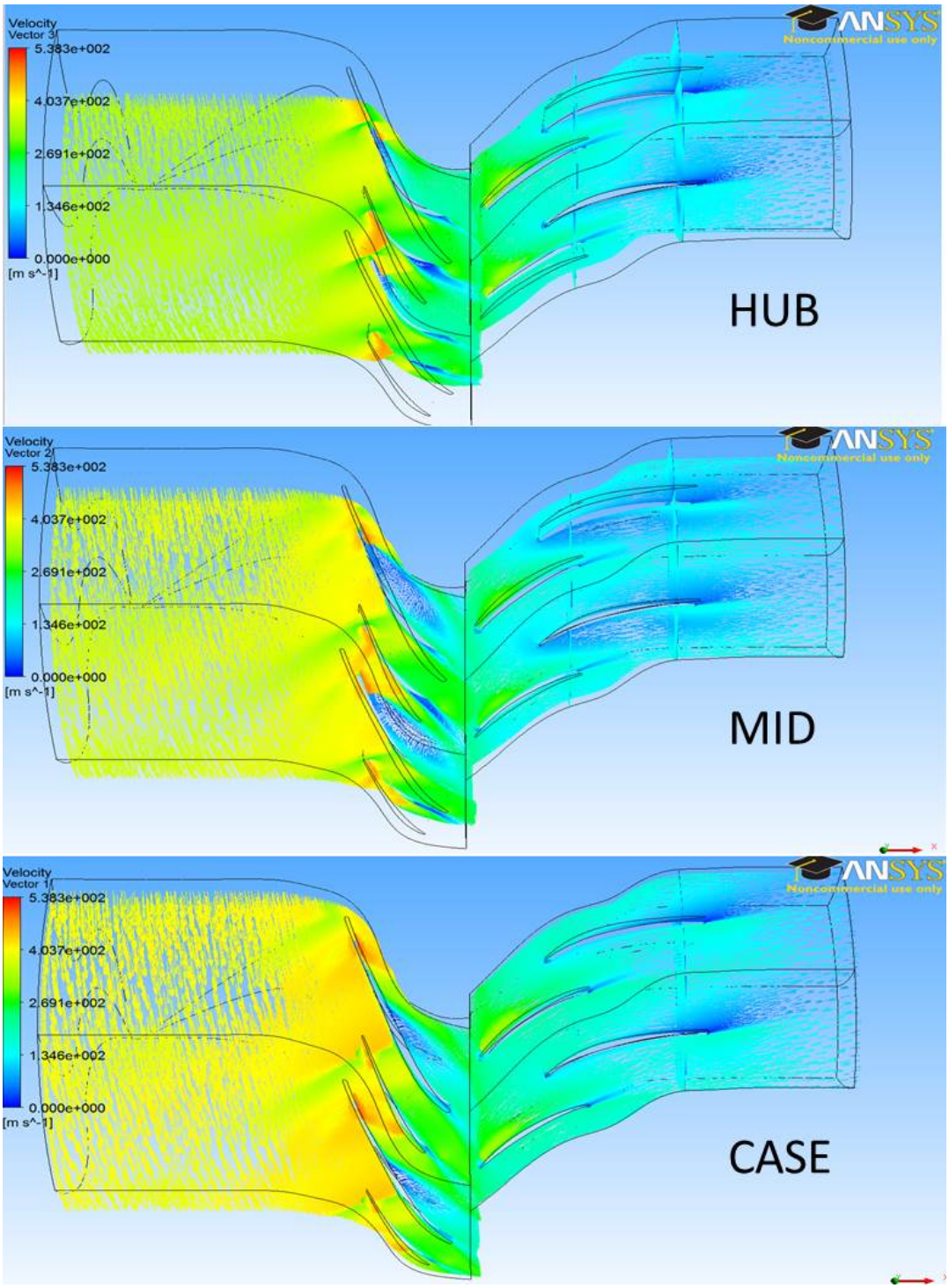

Figure 8. Flow Visualization at different radial height

1. Effects of Blade Offset

The majority of blade design efforts involved manipulating the camber of the LB and TB. The blade offset parameter defined in Appendix A Table 1, was initially used to ensure the blades did not physically overlap when drawn on the stator hub and had some moderate separation between LB suction surface and the TB pressure surface. While an arbitrary distance was adequate for initial design, subsequent iterations showed the value of varying blade offset to produce a local "aerodynamic throat" that would reenergize the flow and produce a delay in flow separation. Figure 9 shows the relative effects of various offset inputs. The final design offset was 0.8 of the passage width, with the hub at 0.85 and tip at 0.87. Of note, while -0.25 and 0.75 offset should be identical, care must be taken when using the algorithm used to draw the air wedge. It can produce incorrect shapes for some input parameters. Choosing the alternate input will resolve any geometry issues.

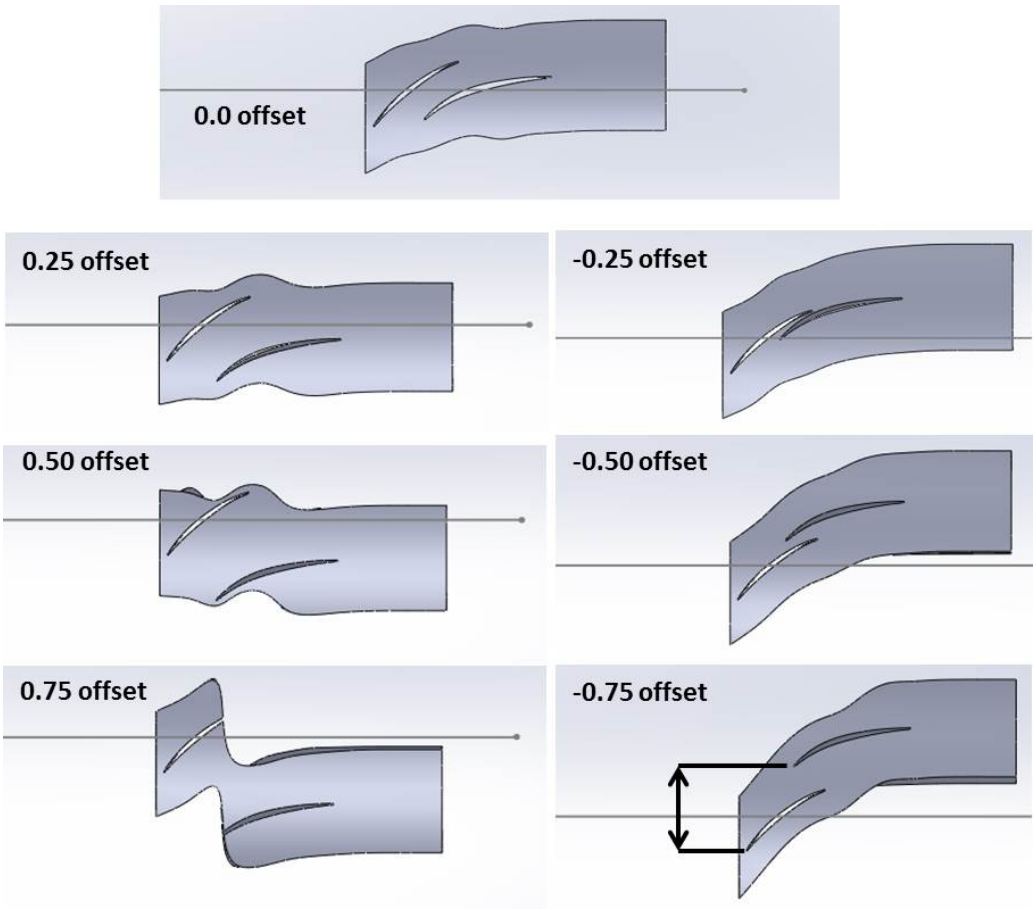

Figure 9. Stator blade offset geometries

2. Bowed Blade Ends

Flow separation and vortex generation in the blade-casing and blade-hub interface regions is the last hurdle in producing a well behaved and efficient flow field at the target mass flow. As discussed by Vavra [6], Breugelmans et al. [7], and Sasaki and Breugelmans [8], wall boundary layer buildup and blade corner region interaction can be controlled with dihedral or lean angle. Bowing the blade at both casing and hub can reduce the losses due to suction surface flow separation. Figure 10 shows the wakes of the stator blades with and without blade bowing for the same back pressure.

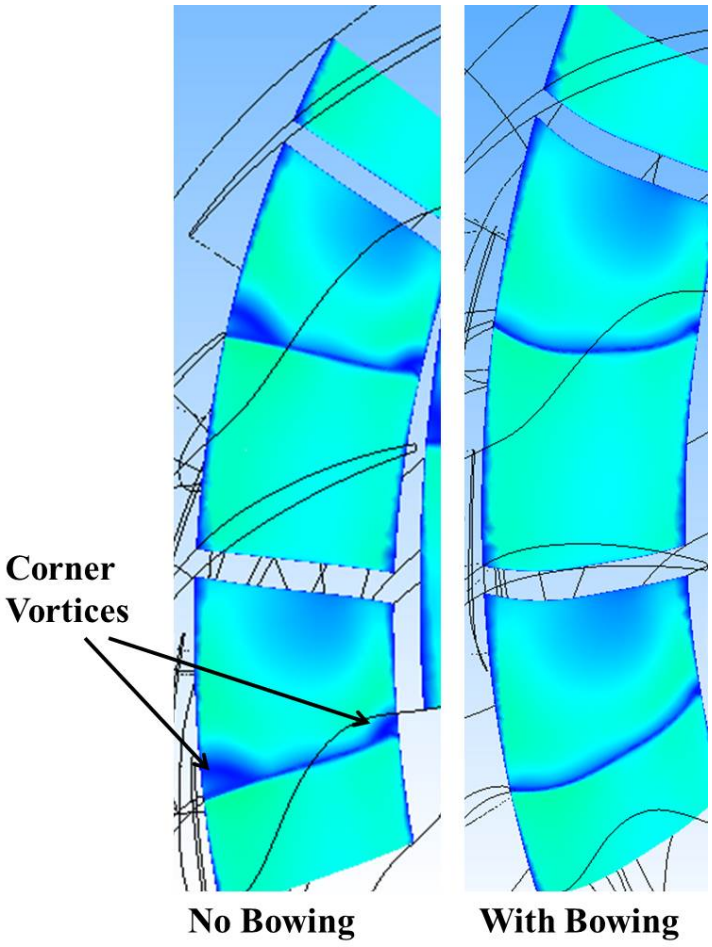

Figure 10. Stator blade wakes showing the effect of bowing

THIS PAGE INTENTIONALLY LEFT BLANK

III. EXPERIMENTAL FACILITY AND PROCEDURES

The rotor was tested in the TCR facility at the NPS TPL. The TCR layout was as designed by Dr. M. H. Vavra, and as described by McNab [9] with the exception of those modifications described in Drayton [1].

This chapter describes the modifications required to install the redesigned rotor casing, the stator, the experimental procedures followed for data collection, and the data acquisition and reduction methods.

A. ROTOR ONLY TIP GAP MODIFICATIONS

1. Transonic Compressor Rig

A detailed description of the compressor rig installation is included in Drayton [1]. The TPL transonic compressor rig (TCR), Figure 11, includes a casing ring, AS2 as depicted, which is designed to contain blades in the event of failure, provide instrumentation portals, and provides a mounting surface for abradable tip gap sealing material in the form of a radially wider inner channel corresponding to the rotor blade tip path. As rotor speed increases, the blades will radially elongate and contact the abradable material. The blade tips behave like a cutting edge and machine the abradable surface until a minimal TG is achieved. This behavior would be present at ever increasing rotor speeds thus maintaining a small TG on initial testing. Subsequent testing would obtain optimal (minimal) tip gap distance only at full operating speed, which is typical of actual engine design and operation.

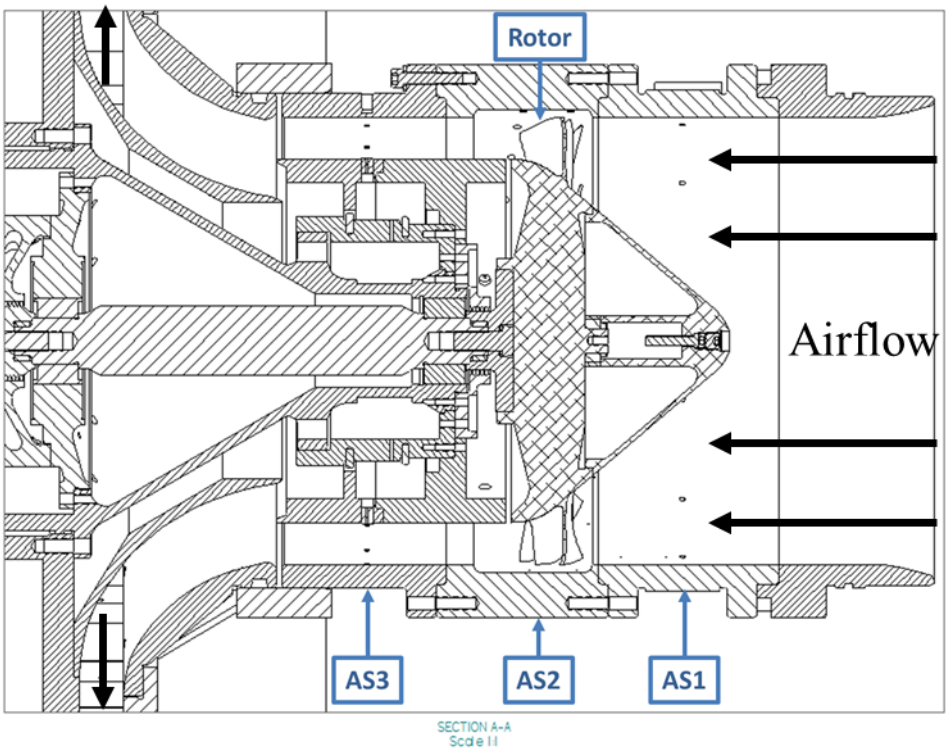

Figure 11. TCR cross-section with the TASR installed (after [1])

2. Initial Rig Mounting Design and Changes

Initial design of the rotor and TCR interface proved to be inadequate. To attach the rotor to the TCR, the rotor downstream face was machined with a raised lip surrounding the mounting bolt holes. The interface is shown in Figure 12 with overall components shown in Figure 13. Initial design and manufacture specified a relatively loose fit, with a 0.0381 mm (0.0015 in) clearance between rotor mounting race and mounting flange. This loose fit coupled with low, but within specification, mounting bolt torque produced a catastrophic failure. At operating speeds, the loose fitting flange caused mounting bolts to stretch that increased rotor and shaft separation, which increased vibration. This increased vibration allowed blade tips to impact the rotor casing and remove large sections of the abrasion strip, which then fouled the passage and precipitated the failure of the rotor blades.

Figure 12. Rotor downstream face and new mounting flange

These failure investigations lead to an increase in flange diameter for an interference fit as part of the redesign of TCR shaft mounting. The interference fit can be seen in figure 12. The rotor shaft was assembled with mounting dowel pins and the shaft mounting bolts were torqued to new specification, Appendix B. Taking advantage of aluminum's higher coefficient of expansion, the aluminum rotor was heated to expand the mounting race diameter then placed on the steel mounting flange and aligned. Rotor mounting bolts were inserted and torqued to new specification while the rotor continued to cool. This ensured a tight and most importantly a concentric fit. Flange drawings may be found in Appendix C

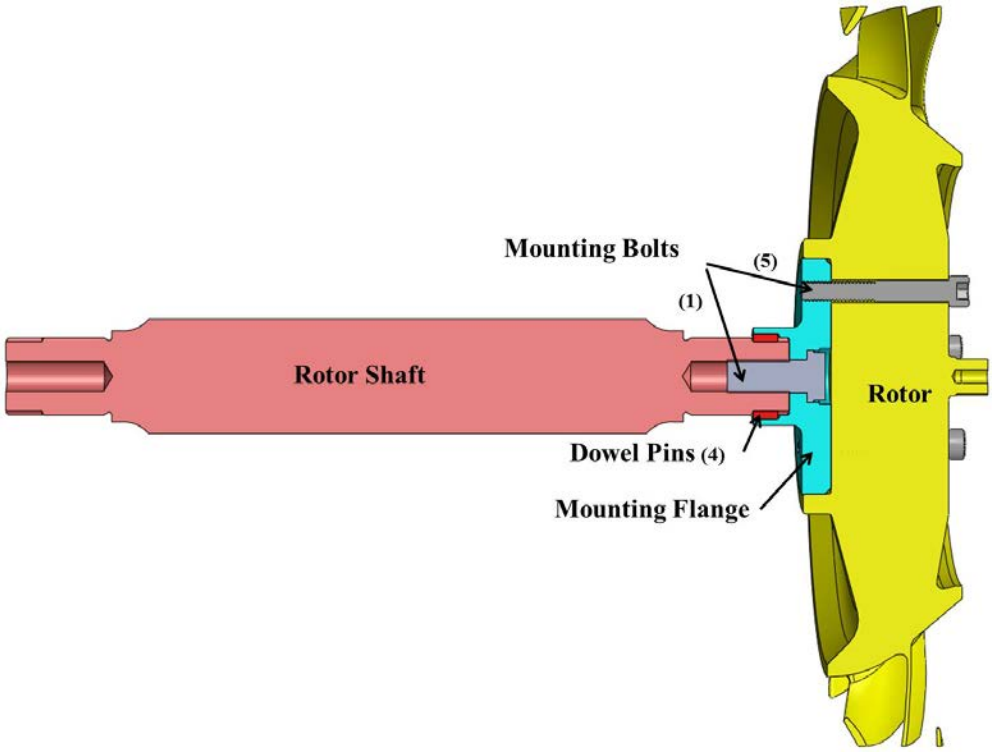

Figure 13. Redesigned rotor shaft interface

3. Current Modifications

With the mounting flange-rotor interface vibration problem addressed, the rotor casing ring, AS2, was redesigned to allow for more ease in varying tip gap and casing treatments. The region that contains the abradable surface was increased to provide greater flexibility in rotor blade length and geometry. Drawings of this design are contained in Appendix D.

Additionally, the Dow Corning one part silicone rubber abradable material chosen for initial rotor experimentation was replaced. Initial testing with this material installed in the casing ring yielded catastrophic results as abrasion characteristics were not predictable. The Dow Corning compound was retained but machined to increase TG according to Drayton's [1] description. This increased tip gap allowed initial collection of performance data on the remaining TASR. With unsatisfactory characteristics and performance suffering from the increased TG, West Systems 105 epoxy resin, 209 extra slow hardener, and 407 low density microballoon filler or 410 microlight filler replaced

the Dow Corning product, Figures 14 and 15. The West System product demonstrated predictable and benign fracture and abrasion characteristics. Test pours were prepared using a 5/1 ratio of epoxy to hardener with the addition of filler to desired consistency. The 410 microlight filler (cream color) was chosen over the 407 low density filler (maroon color), Figure 15. The 410 filler is constructed with smaller particles and abrades in a manner akin to sanding, while the 407 filler produced larger particles and tended to fracture in a less desirable fashion.

Figure 14. West System epoxy and hardener

Figure 15. West System filler additives

The initial TG will be 0.711 mm (0.028 in) cold and 0.355 mm (0.014 in) at 27000 rpm or 100 percent maximum operating speed.

B. TRANSONIC COMPRESSOR RIG AND ROTOR INSTALLATION

1. Compressor Installation and Instrumentation

The rotor was installed according to Drayton [1], with modifications to the abradable section of the casing and mounting hardware as described previously.

2. Measurement Devices

Stagnation temperature and stagnation pressure probes collected steady-state measurements in the flow field. Unsteady measurements were collected by static pressure transducers installed in the casing. The steady-state probes used were of the same types as described by McNab [9], 1.59 mm (1/16 in) “miniature head” Kiel probes and 3.18 mm (1/8 in) “Standard Head” combination Kiel/thermocouple probes. A

through description of the Kulite instrumentation can be found in Londoño [10]. The characterization of transient data was not part of this study

3. Instrument Placement

Instrument placement was as described by Drayton [1]. Inlet conditions were measured at the AS1 section, Figure 11, with two Kiel/thermocouple and two static pressure probes. Outlet data was gathered at the AS3 station using nine Kiel/thermocouple probes, 11 Kiel pressure probes, two static pressure ports in the rotor casing and four static pressure ports in the TCR hub. Hub and casing temperature were also collected.

The rotor segment, AS2, housed eight Kulite Miniature IS Pressure Transducers in a 15 degree stagger about the casing radius at increasing axial distance from the upstream face as depicted by the ports in Figure 16. In addition to the eight pressure transducers, 16 static ports were included in a similar stagger-axial shift arrangement.

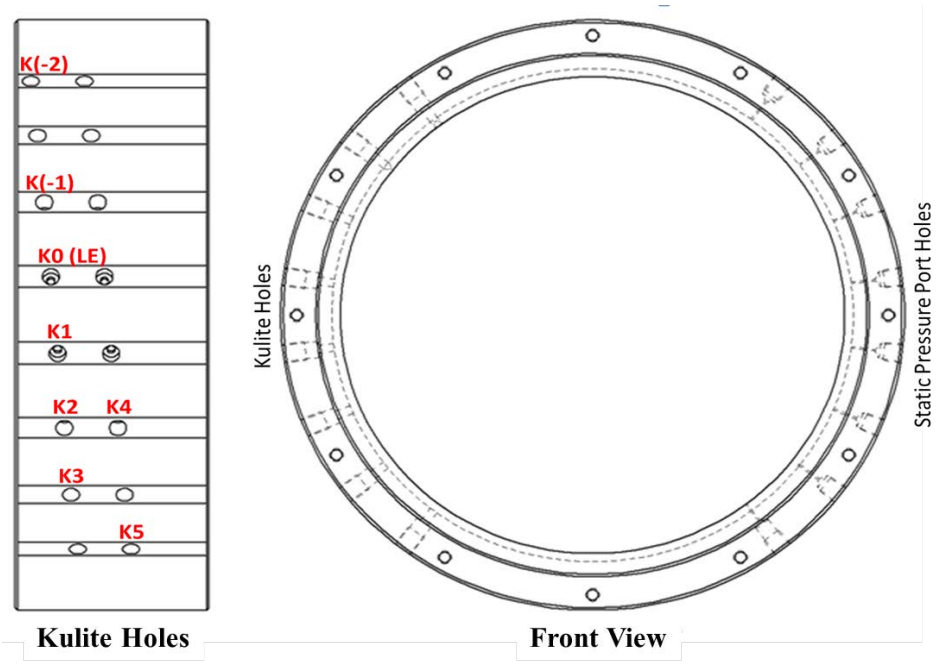

Figure 16. Kulite and static port arrangement

C. FINAL STATOR DESIGN

The original TCR design allows for modification in an axially modular fashion. The stator stage was rendered as a complete blisk in SolidWorks and then modified for incorporation into the TCR. The blisk was split into two rings as depicted in figure 17. The forward two-thirds of the lead blade is fixed to the upstream ring with the remaining portion of the blade overhanging the trailing blade ring. The trailing blade is wholly supported by the trailing ring. This two ring arrangement allows for the "clocking", as in Figure 9, of the stator to investigate the relative performance effects of lead-trail blade offset. Once the separate rings are defined, the inner portions of the rings are modified to fit on the TCR stator support structures.

Figure 18 displays the stator support structure, a non-rotating structure within the TCR that supports the addition of downstream stator assemblies. Also shown are "blank" rings that would be mounted downstream of a rotor if a stator was not included in the current testing phase. These blank rings were remanufactured, including the hybrid stator stage and allow for the trail ring to remain fixed in relation to the rig while the lead ring can be mounted at different offset angles. The lead ring is then fixed in position and the remaining sections of the TCR are mounted and the rig is prepared for operation Figure 19. Stator drawing can be found in Appendix E.

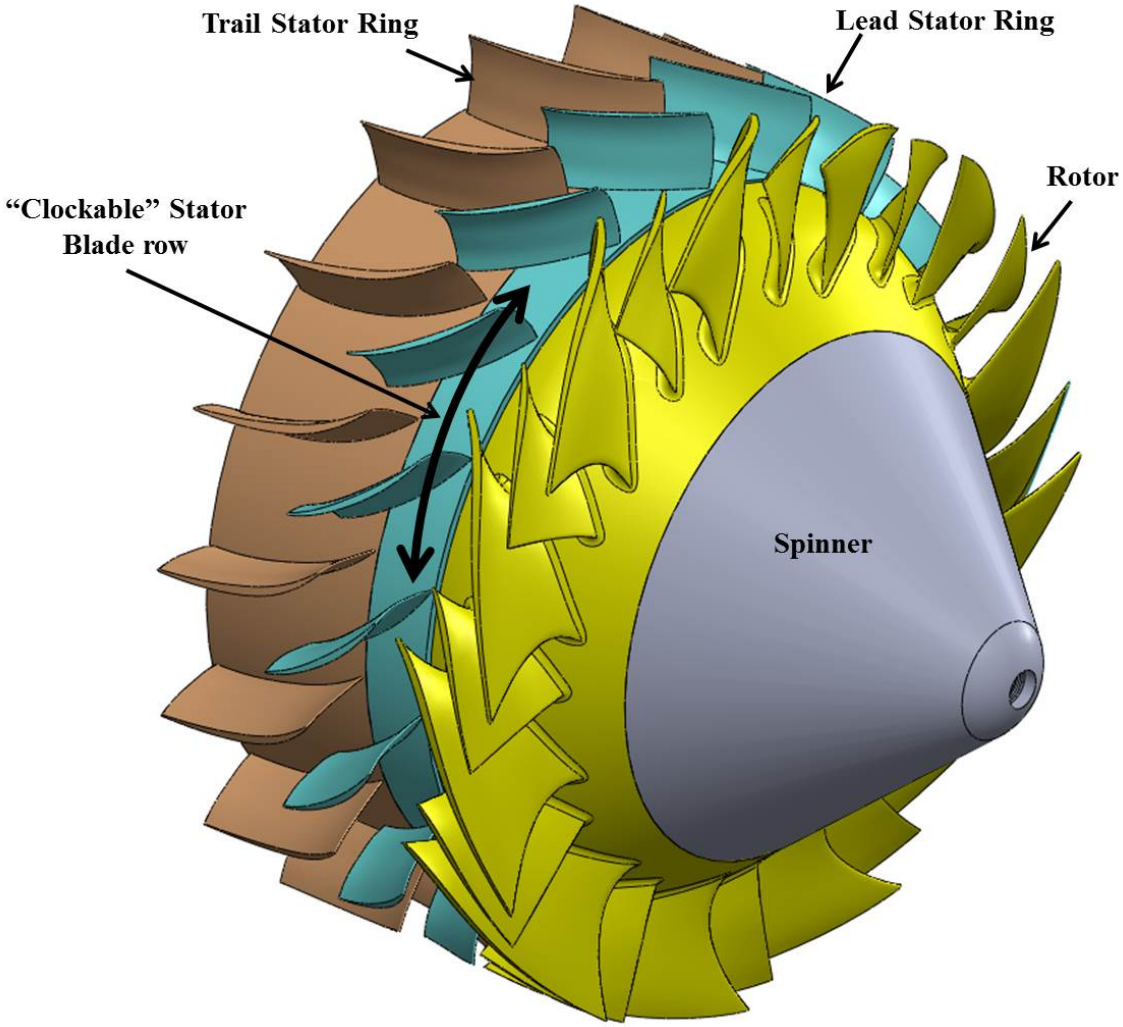

Figure 17. Two ring arrangement of hybrid stator with rotor and spinner

Figure 18. Stator Support Structure and “Blank” Stator Rings

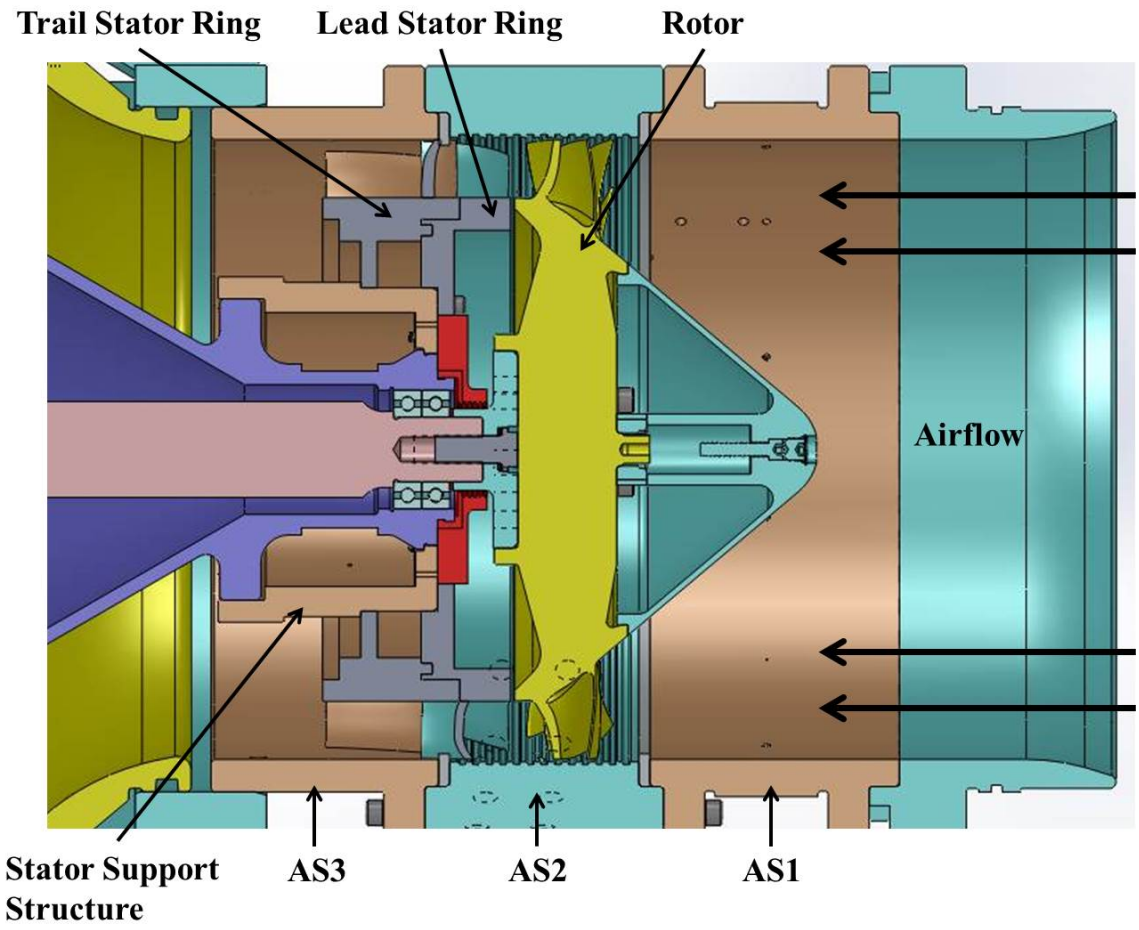

Figure 19. TCR cross section with rotor and stator installed

D. EXPERIMENTAL PROCEDURE

TCR configuration and operation are described by Grossman [11] but for completeness will be summarized. The test article was powered by two opposed rotor, single stage air-operated drive turbines mounted on a common shaft as shown in Figure 20. These turbines received air from a 12-stage Allis-Chalmers axial compressor capable of providing 2.2 kg/sec mass flow rate with a maximum of 2 atmospheres gage pressure. The test compressor was connected to the drive turbines via the redesigned shaft discussed previously. An air-operated balance piston was located between the compressor shaft and the test compressor to counteract the axial forces exerted during operation and reduce bearing stresses. Compressor speed was controlled via an electronically actuated butterfly valve that was used to throttle the air supply to the drive

turbines. Airflow to the rig was controlled using an electromechanical actuated rotating plate throttling valve and settling chamber. Mass flow rate through the test article was measured by a flow nozzle positioned downstream of the settling chamber

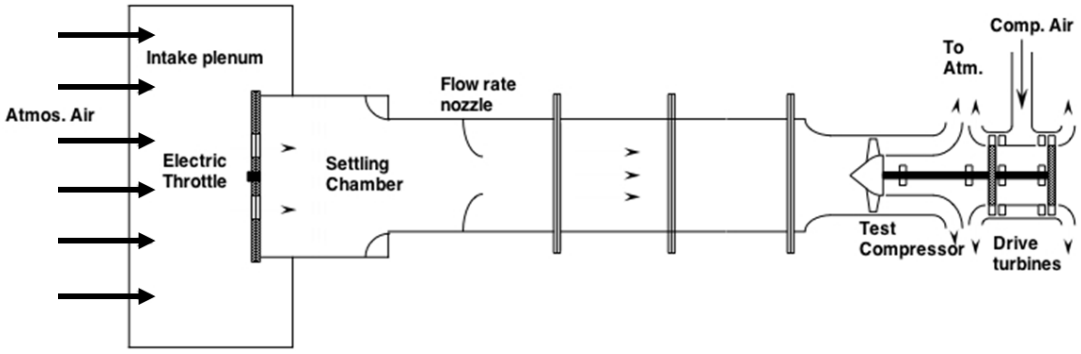

Figure 20. TCR configuration after Drayton[1]

Every experimental session began with the start and warm-up of the Allis-Chalmers compressor, introducing air to the balance piston, and initiation of lubrication oil to the bearings via an air driven oil mist system. A pre-test checklist is provided in McNab [9].

Each experimental run produced one speed line. Testing began by throttling the drive turbine supply air to produce a corrected rotor speed that accounted for daily atmospheric conditions. The correction ensures that the rotor runs at the correct tip Mach number. Acceptable corrected speed was within a fraction of one percent of the desired speed. Data collection began with the upstream electric throttle valve in the open position. The valve was closed in varying increments to reduce the air mass flow through the TCR. Throttling increments were varied to reflect the operating regime. Beginning with large steps, the incremental steps decreased to the finest changes possible with the installed hardware as the rotor approached predicted stall conditions. At each throttle position, data measurements were recorded and cross-checked with the CFD-derived performance maps.

E. DATA COLLECTION AND PROCESSING

Steady-state data was collected using the existing TPL data collection system. An HPVEE data acquisition program developed by Gannon [12] and described by McNab [9] measured the TCR steady-state pressures and temperatures. For completeness, a brief description is given. The HPVEE software was installed on a PC that controls a HP Mainframe, which recorded measurements from temperature, pressure and rotational speed instrumentation. Pressure probe monitoring is achieved through three ScaniValve pressure bricks. The HPVEE program calculated mass averaged stagnation pressure, temperature, and isentropic efficiency through mass averaging the temperature and pressure data, Hobson et al [13]. Four data points are collected for each operating point at approximately two-second intervals.

The unsteady data was collected from the Kulite Miniature IS Pressure Transducers located in the rotor segment (AS2) using a DAC Express data acquisition system described by Londoño [10]. All probes were calibrated before each data collection run using 0.2 second samples for successive known backpressures applied to the backside of the probe. During testing, 20 second samples at a speed of 196.608 KHz were recorded on the system's mainframes for different flow and operating conditions resulting in over a half a million data sample points. Data files were saved in a comma delimited form (*.csv) for Microsoft Excel and processing in MATLAB. Code developed by Londoño [10] was used to reduce the data. Each rotor blade passage was divided equally using 100 points. Blade passage mean pressures were transformed into a pressure distribution map by taking all the Kulite pressure signals at each of the points across the blade passage to produce the smooth mean. The final contour plot was formed by sequentially joining and interpolating the pressure averages for each Kulite data set Gannon [12], which matches experimental data, Figures 21 and 22.

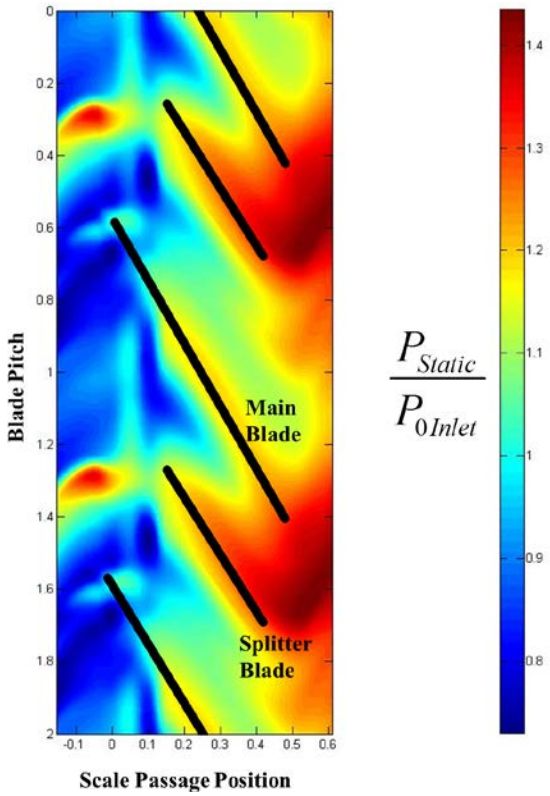

Figure 21. Experimental rotor pressure contour plot with improved post processing

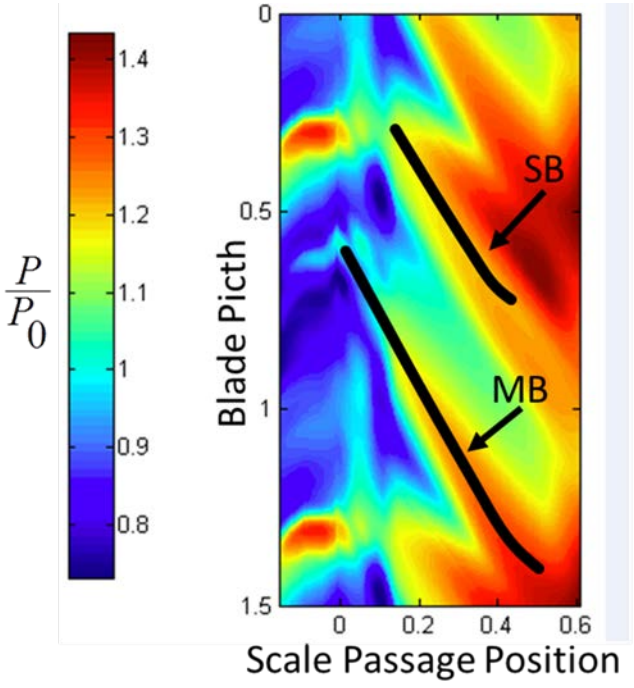

Figure 22. Experimental rotor pressure contour plot(after [1])

IV. RESULTS

A. ROTOR TIP GAP REDUCTION

Drayton [1] conducted tip gap studies at various design speeds and tip gap distances. As previously discussed, problems with the rotor dynamics and abradable material led to investigations with less than optimal tip gap distances. Numerical investigation were conducted with cold shapes and calculated hot tip gap distances. Blades are calculated to grow in length 0.36 mm (0.014 in) at 100 percent (27,000 rpm) design speed due to dynamic forces.

Figures 23 and 24 show numerical and experimental data for 0.254 mm (0.010 in) and 0.914 mm (0.036 in) tip gap respectively.

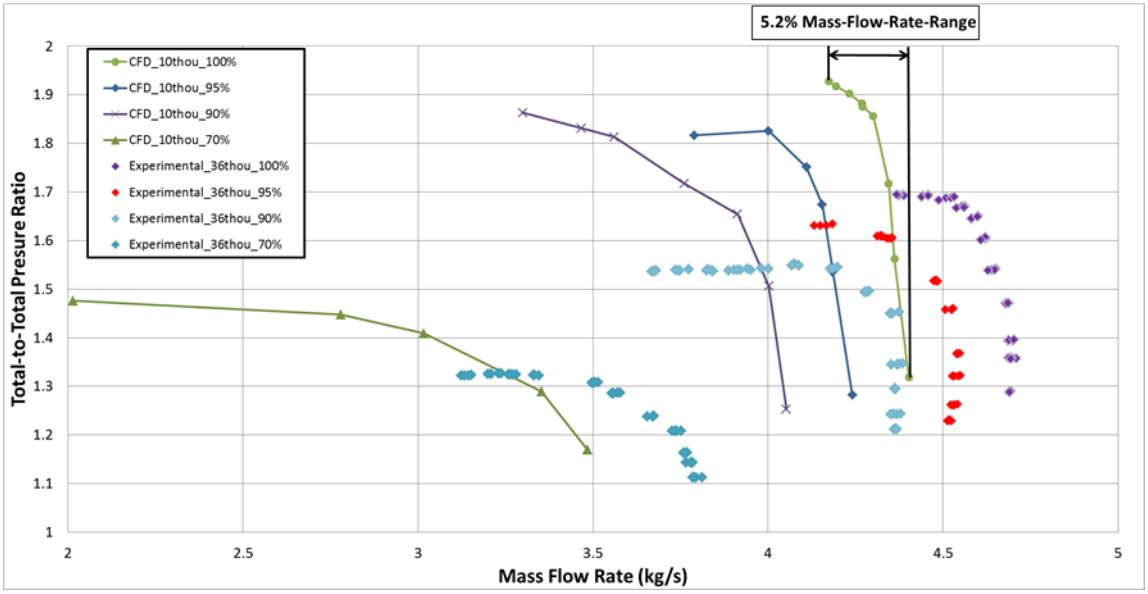

Figure 23. Rotor pressure ratio versus mass flow (after [1])

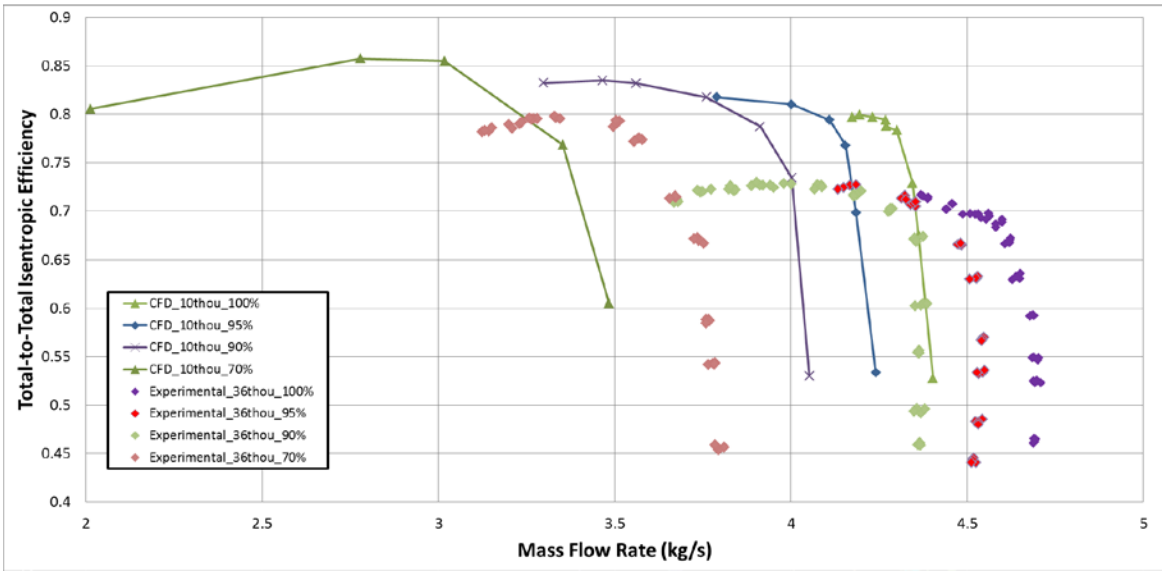

Figure 24. Rotor efficiency versus mass flow (after [1])

Rotor performance at the large experimental tip gap is well below that of the calculated 0.254 mm (0.010 in) design goals. Additional experimental investigations at 60 percent speed showed that performance from a 0.914 mm (0.036 in) gap was considerably improved when tip gap distance was lowered, Figure 25. The maximum pressure ratio increased to 1.28 from 1.23 and the mass flow rate range increased from 23 percent to 25 percent.

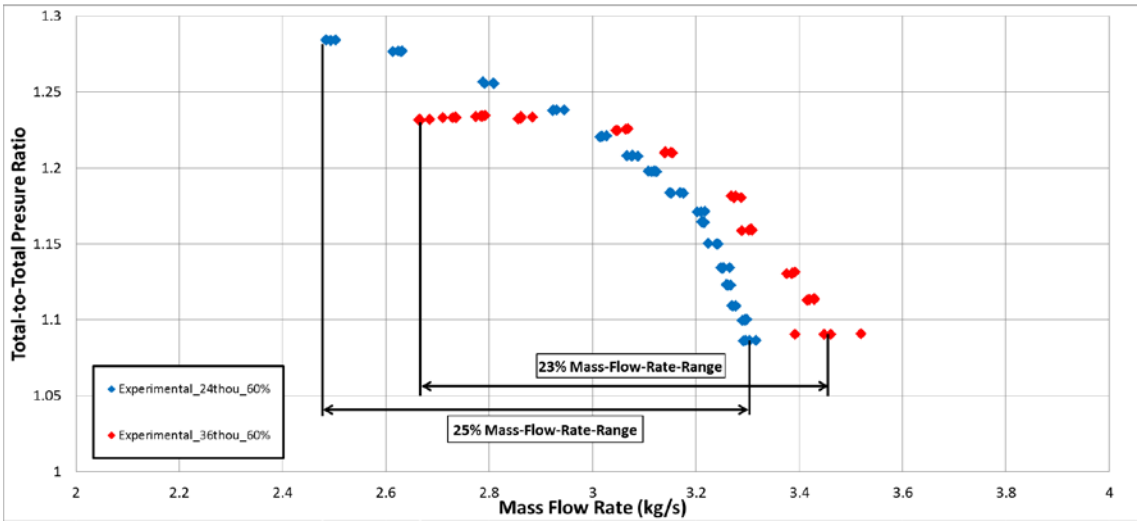

Figure 25. Experimental pressure ratio versus mass flow for decreasing tip gap (after [1])

Experimental and numerical power absorbed by the rotor is shown in Figure 26.

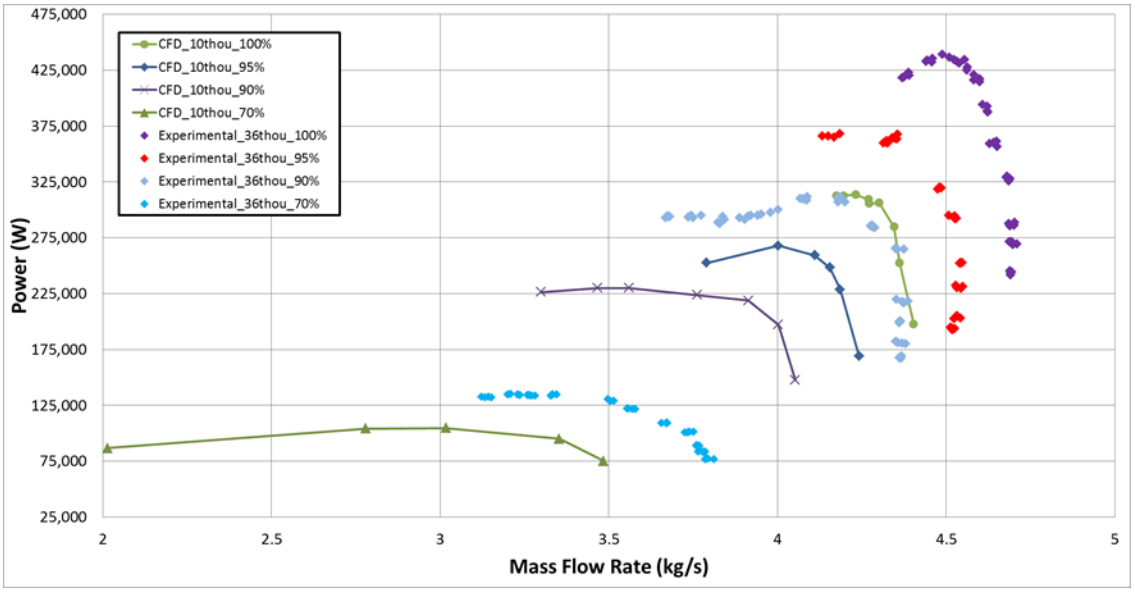

Figure 26. Rotor experimentally versus numerically determined power map (after [1])

B. ROTOR-STATOR PAIR

Baseline rotor-stator performance is shown in Figure 27. Maximum predicted performance figures are 1.97 (76.7 percent) pressure ratio and 77.5 percent (PR=1.94) efficiency. The stage was evaluated with no tip gap over the rotor and at 70 percent, 80 percent, 90 percent and 100 percent operational speeds, as shown in Figure 28. The pressure ratio and efficiency curves both display like characteristics and the same trends as the rotor only performance map with a slight loss in peak efficiency, Figure 29, and a slight gain (+0.05) peak pressure ratio and predicted mass flow rate range, 8.4 percent versus 5.3 percent.

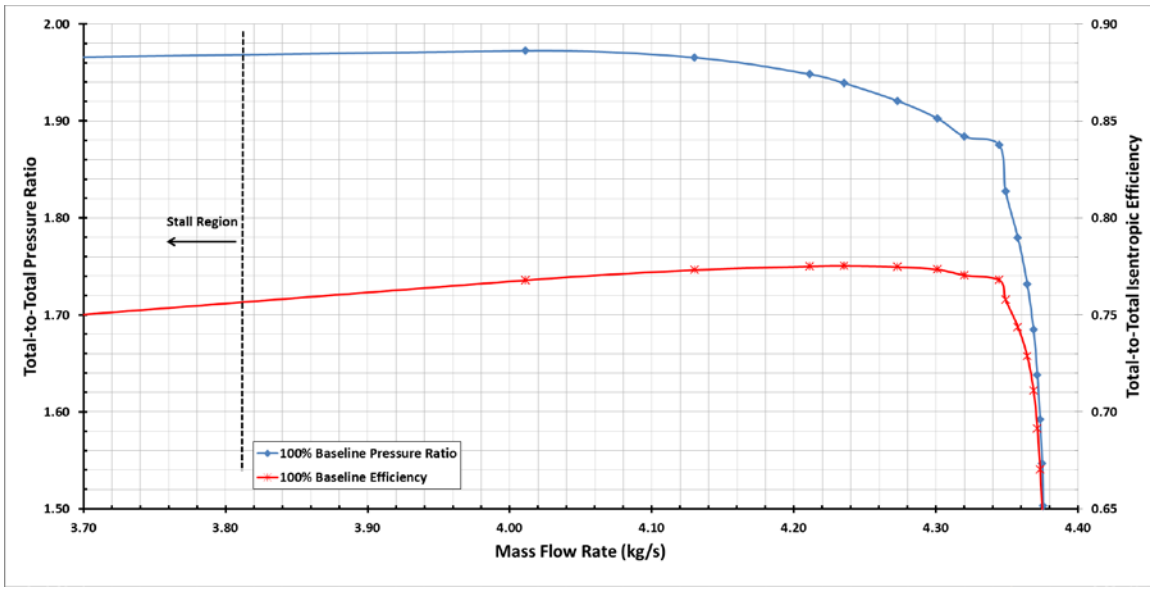

Figure 27. Baseline rotor-stator pressure ratio (left axis) and efficiency (right axis)

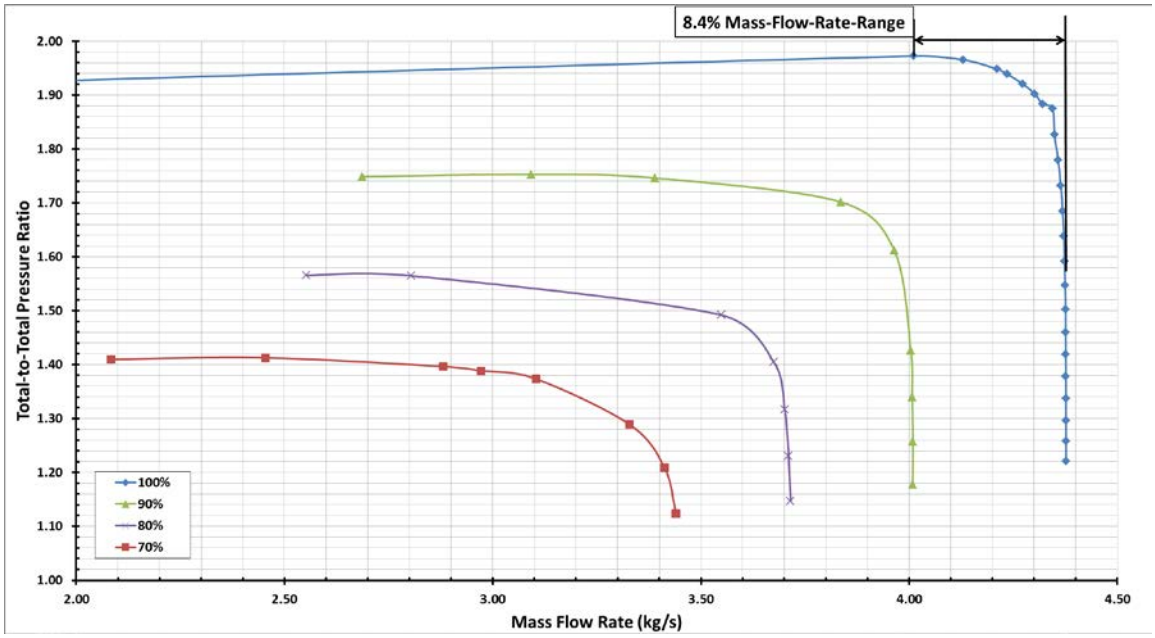

Figure 28. Pressure ratio at various operating speeds

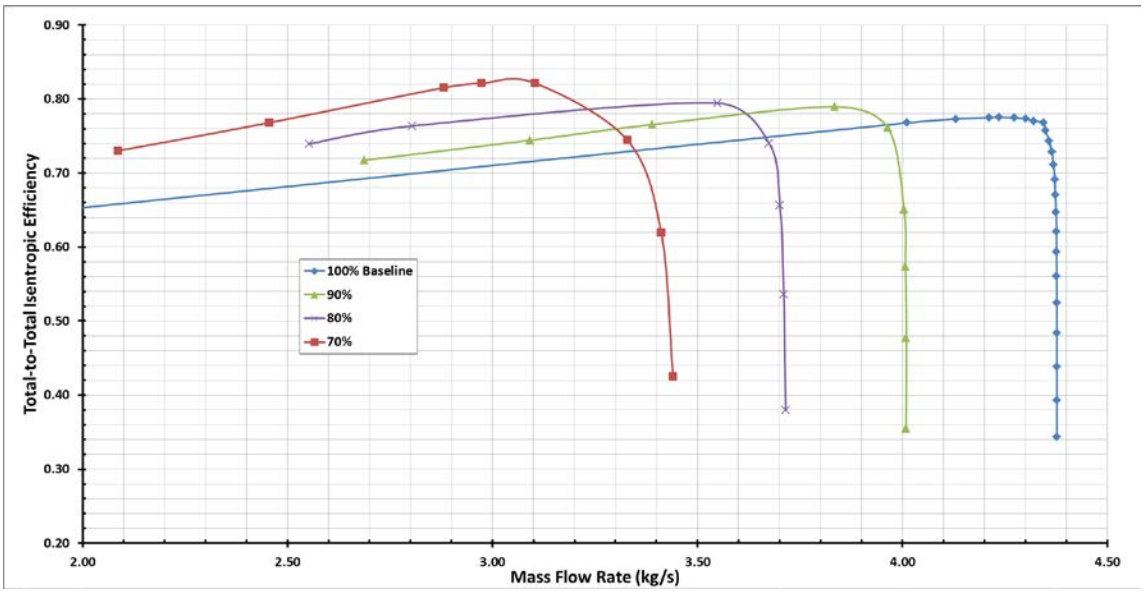

Figure 29. Efficiency at various operating speeds

The computed power map for the rotor and stator is shown in Figure 30. For nearly the same mass flow rates, the stage displays slightly lower numerically derived power absorbed than the rotor only configuration at 331 kW vs 339 kW as expected due to the lower computed stage efficiency.

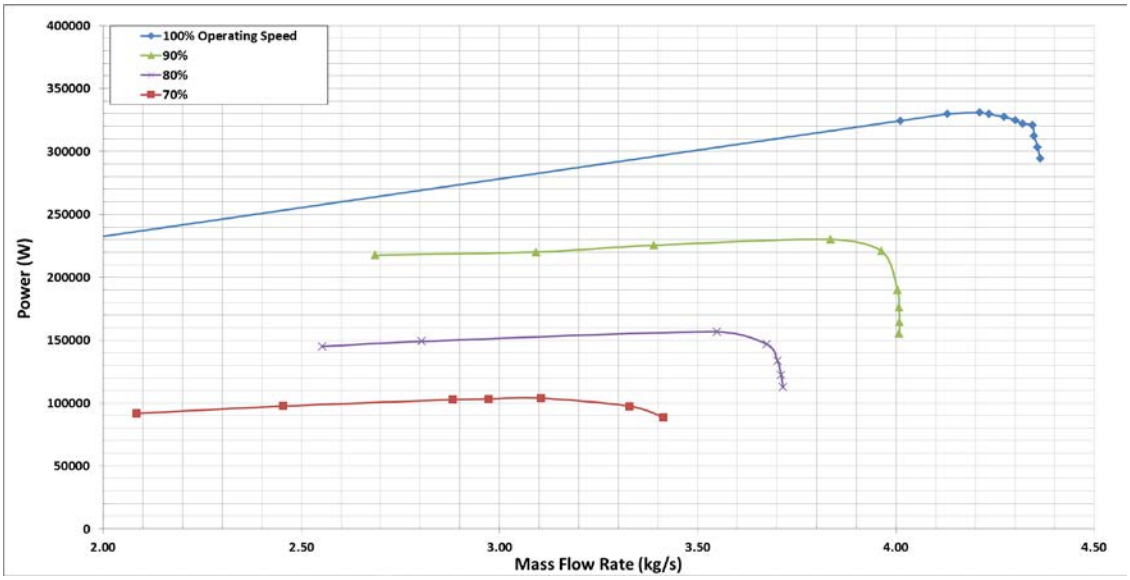

Figure 30. Power at various operating speeds

Additionally, a study to understand the effects of varying the offset between blades was performed. With the baseline stator design offset distance as the control location, air wedges were created by perturbing the trailing blade some distance toward and away from the leading blade. Figure 31 displays the perturbation nomenclature as it relates to the stator. Perturbations from 15 percent of the original distance to 25 percent were conducted.

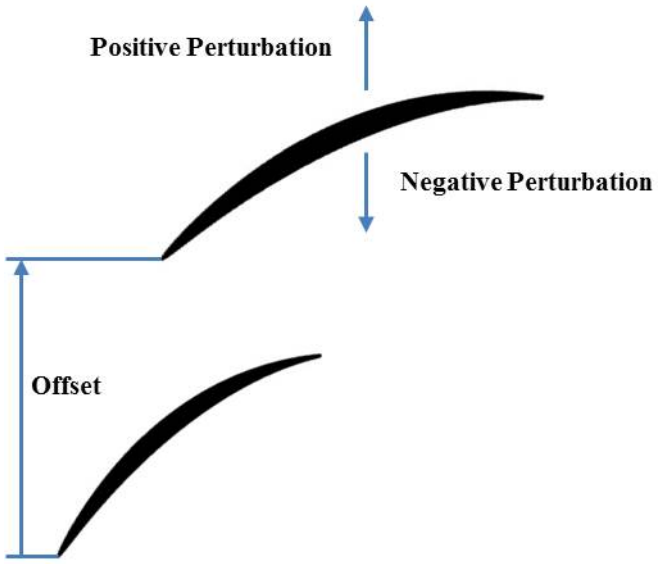

Figure 31. Offset perturbation

Though the peak data for positive perturbation in Figure 32 not as behaved as the baseline data, a trend can be observed. For an increased distance between the stator lead and trailing blade there is increased pressure ratio over the baseline design. Unfortunately, the efficiency map, Figure 33, shows that all the perturbed geometries displayed efficiencies less than the baseline design. This is likely due to the fact that the baseline geometry was designed for the baseline offset and not intended to operate at peak performance in off design offset distances.

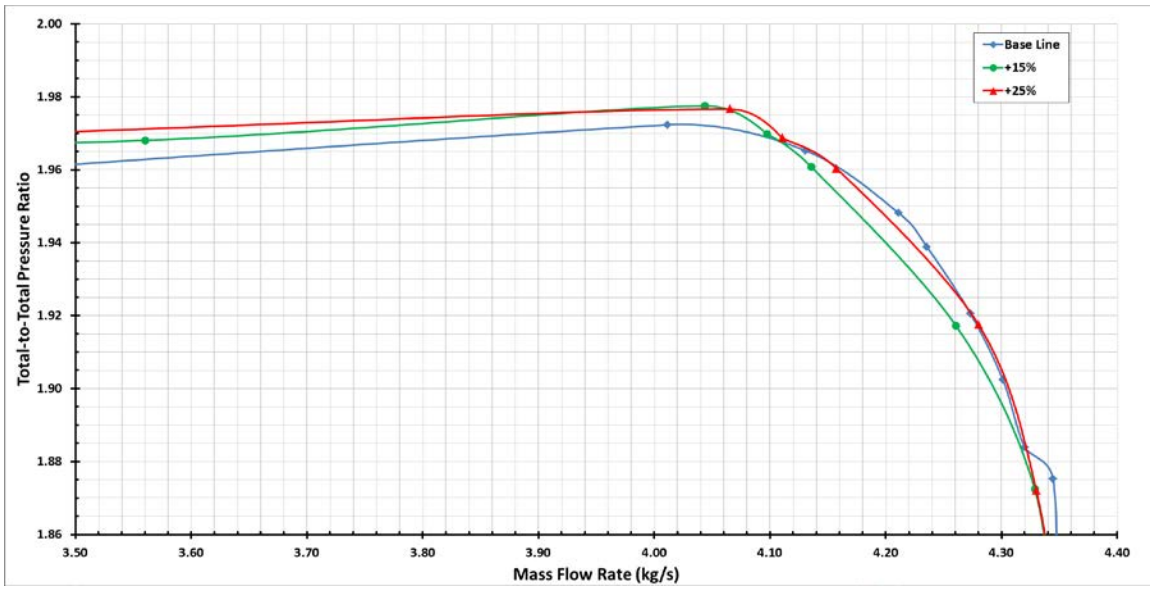

Figure 32. Positive perturbation pressure ratio

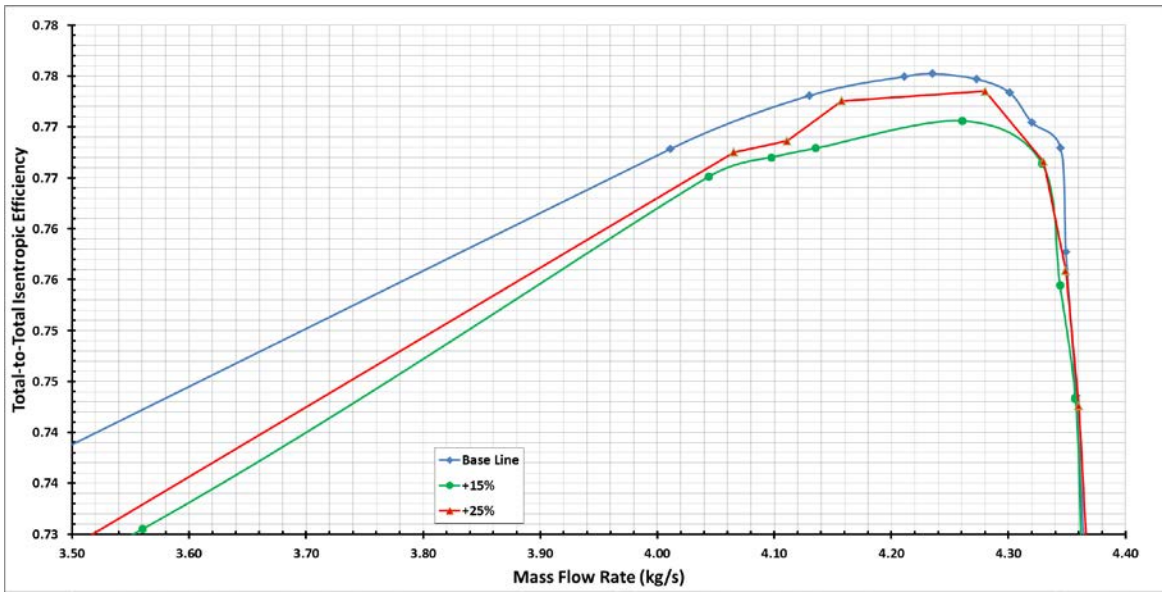

Figure 33. Positive perturbation efficiency map

The negative perturbation pressure ratio and efficiency results are shown in Figures 34 and 35. Unlike the positive perturbation investigations, efficiency increases for a lower pressure ratio as compared to the baseline geometry.

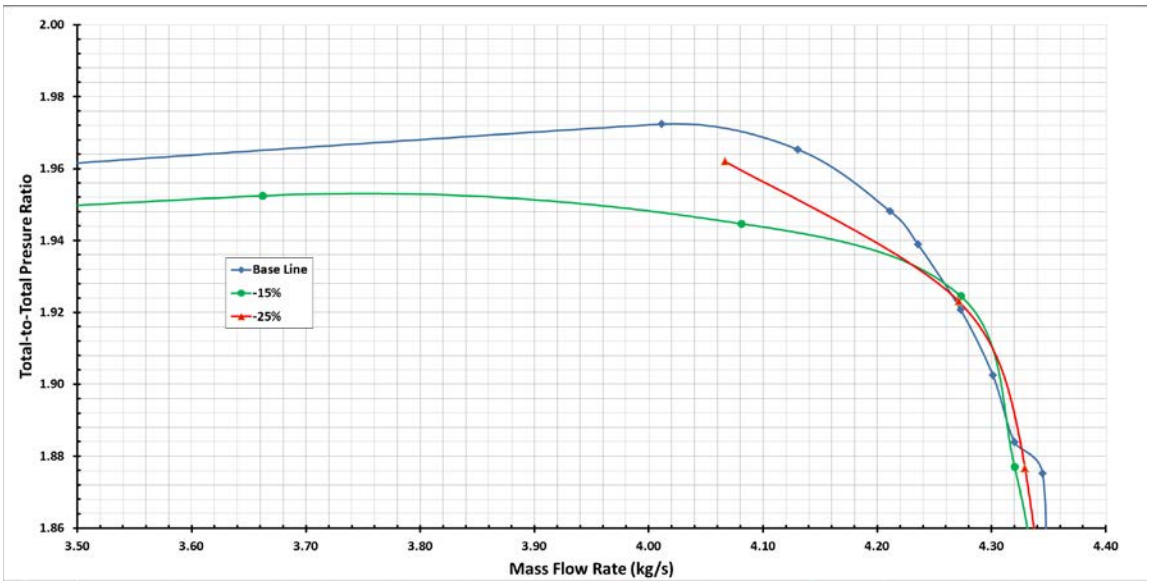

Figure 34. Negative perturbation pressure ratio

Again, opposite the positive perturbation, which displayed high peak and shallow decay as mass flow decreased, the peaks for negative perturbation peak and fall off quite sharply. Of note is the behavior of the "close" geometries, -20 percent and -25 percent, that stall at much lower mass low rates due decreased distance between lead blade suction surface and the trail blade pressure surface.

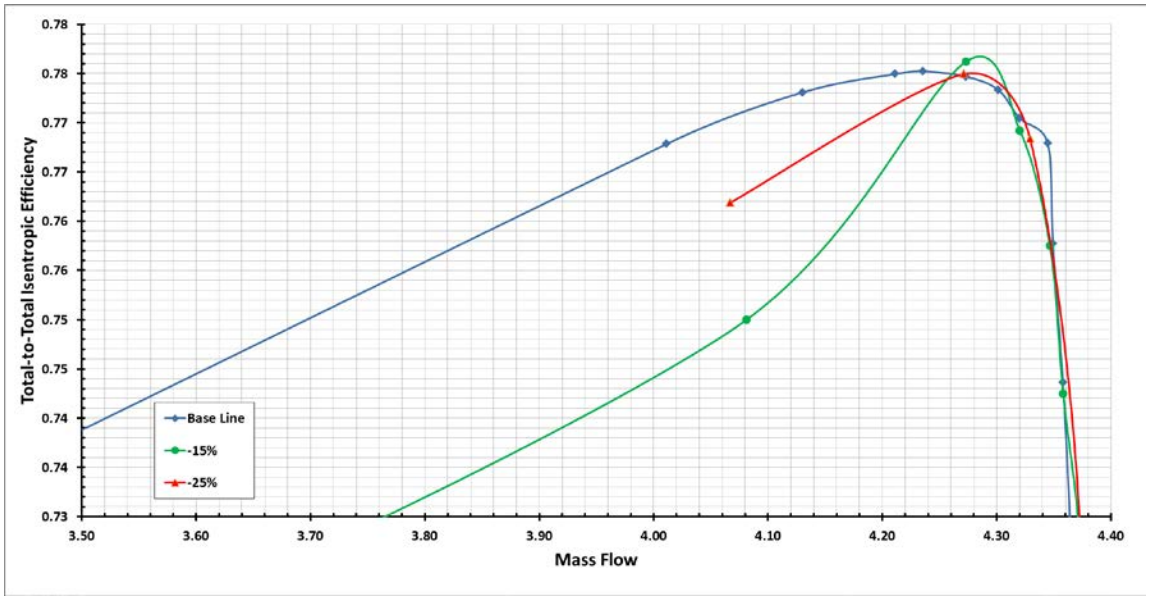

Figure 35. Negative perturbation efficiency map

V. CONCLUSIONS AND RECOMMEDATIONS

A. CONCLUSIONS

Objectives for this study were to design a tandem stator for inclusion behind an advanced transonic splittered rotor. Redesign and modify the TCR to increase reliability, survivability and flexibility. Modify design tools for additional blade rows and design manufacture and test the blade rows with the TASR. In the pursuit of these goals the following were realized.

- The successful modification of NPS TPL design tools for design of stator rows revealed the flexibility of this program implementation. Additionally, unforeseen program features were revealed in the exercising of the design tools beyond their original scope. This “stress testing” has provided invaluable insight into the design process and enabled the TPL to further modify the tools to increase automation in the iterative design process.
- The design and analysis of the hybrid stator advanced the understanding of a previously unexplored geometry configuration. The inclusion of the hybrid stator completes the splittered rotor stage and demonstrated the performance gains associated with these novel designs. The investigation and inclusion of offset and blade bowing in the stator design increased stator design knowledge and will allow increased performance when further modified for follow on geometries. The two ring configuration of the stator will allow for extensive investigations that will enable an increase in knowledge of the effects of relative blade offset on stator and overall stage performance.
- The redesign of TCR rotor interface and casing will enable the NPS TPL to test a larger range of compressor geometries. The failure analysis process allowed for greater understanding specific dynamics associated

with the transonic compressor rig. This increased understanding and lessons learned will enable success in future testing at all NPS laboratories.

- The decreased tip gap and new abrasion material should increase the rotor only performance the NPS Transonic Axially Splittered Rotor. The performance increases predicted by the more operationally representative tip gap distances promise to increase TASR performance to new state of the art levels. The additional understanding of splittered rotor characteristics will inform further designs to culminate into operational implementation.

B. RECOMMENDATIONS

Follow on studies should use this work as a base and expand on it as follows:

- Develop an experimental performance map of rotor only configurations with decreased tip gap using the redesigned rotor casing and the new abradable material chosen above. Compare this map to the numerical models and validate the performance improvements predicted.
- Develop an experimental performance map of the rotor-stator configuration, with decreased rotor tip gap, using the hybrid stator developed here. Compare this map to the numerical models and validate the performance improvements predicted.

APPENDIX A. BLADE DESIGN PARAMETERS

Table 1. HardCodeBlade parameters (after [1])

Input Parameter Description	Input Parameter Symbol
Number of blade passages around the rotor assembly	Blade.PassNo
Number of blade sections used to generate the blade	Blade.S
Number of points that define half the blade profile	Blade.P
Blade heights at which properties are inputted	Blade.Heights
Blade chords at prescribed blade heights	Blade.Chord
Blade leading edge (LE) shift as a fraction of axial chord at prescribed blade heights	Blade.LE
Blade leading and trailing edge (TE) ellipse characteristics (minor axis/chord, eccentricity).	Blade.Edges
Blade chord control locations	Blade.Controls
Blade stagger at prescribed blade heights and blade chord control locations	Blade.Stagger
Blade element thickness at prescribed blade heights and blade chord control locations	Blade.Thickness
Blade offset representing the fraction of the passage to rotate each blade element (Main blades at 0.0)	Blade.Offset
Blade axial shift for all blades	Blade.MasterXShift
Fillet radius of all blades	Blade.Fillet
Centering feature (Boolean) specifying whether to center the main blade on the hub origin (true) or align the main blade leading edge with the origin (false) before applying the prescribed axial shift	Blade.Center

THIS PAGE INTENTIONALLY LEFT BLANK

APPENDIX B. ROTOR TORQUE REQUIREMENTS

Final torque requirements for rotor attachment to TCR. Bolts as specified in Figure 23 with torques in Table 2

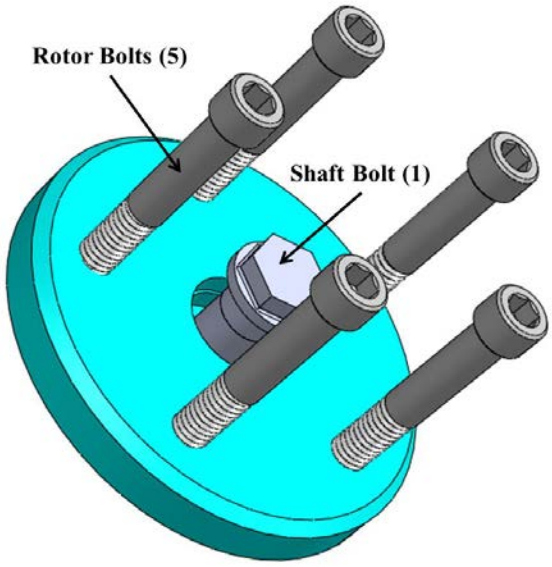

Figure 36. Attachment bolts

Table 2. Torque requirement

	Applied Torques
Shaft Bolt	35 ft-lb
Rotor Bolts	350 in-lb

THIS PAGE INTENTIONALLY LEFT BLANK

APPENDIX C. ROTOR MOUNTING FLANGE DRAWINGS

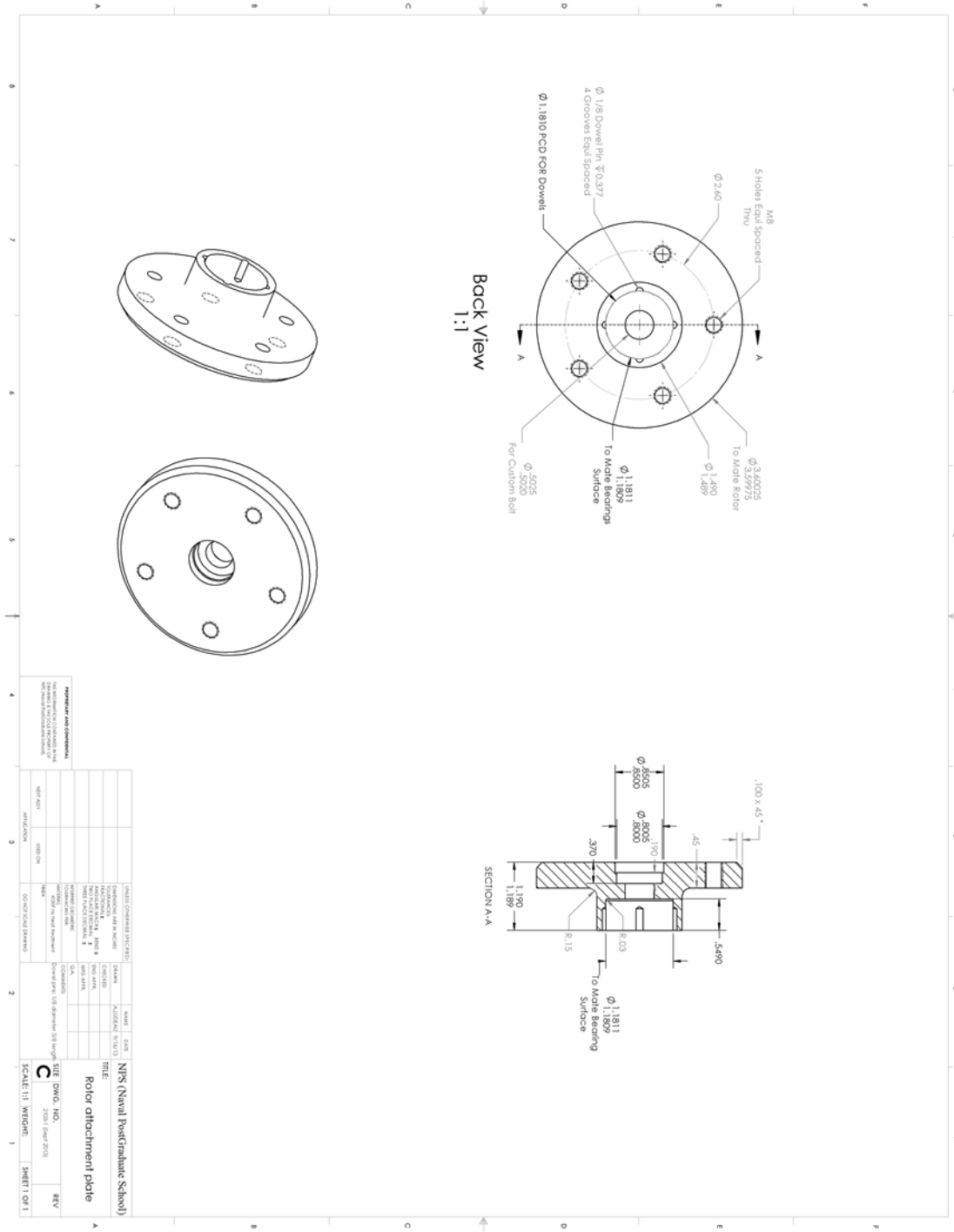

THIS PAGE INTENTIONALLY LEFT BLANK

APPENDIX D. ROTOR CASING DRAWINGS

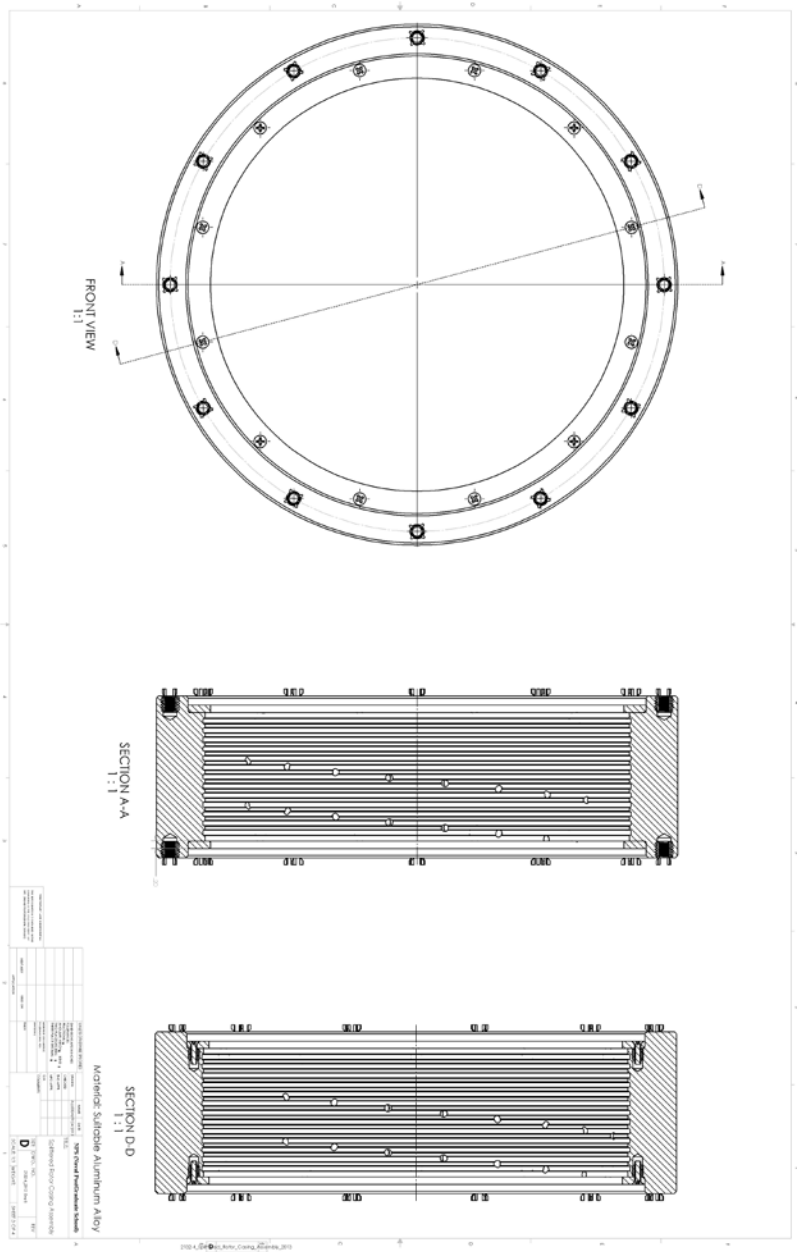

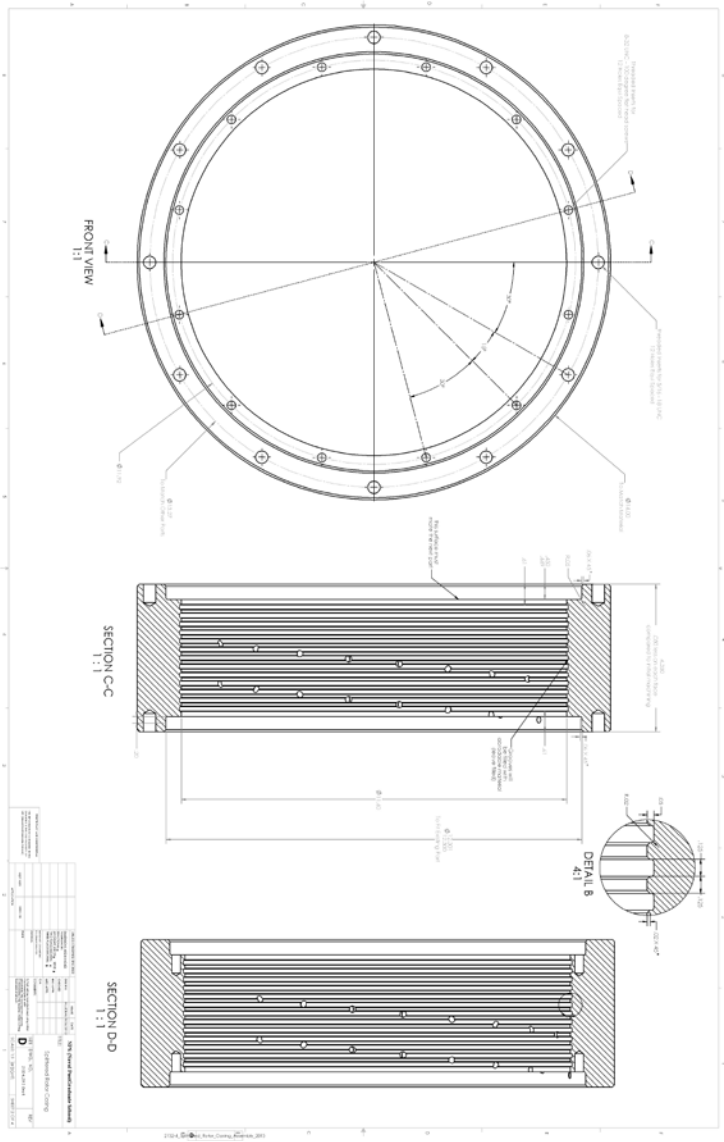
FRONT VIEW
1:1
SECTION C-C
1:1
DETAIL B
4:1
SECTION D-D
1:1

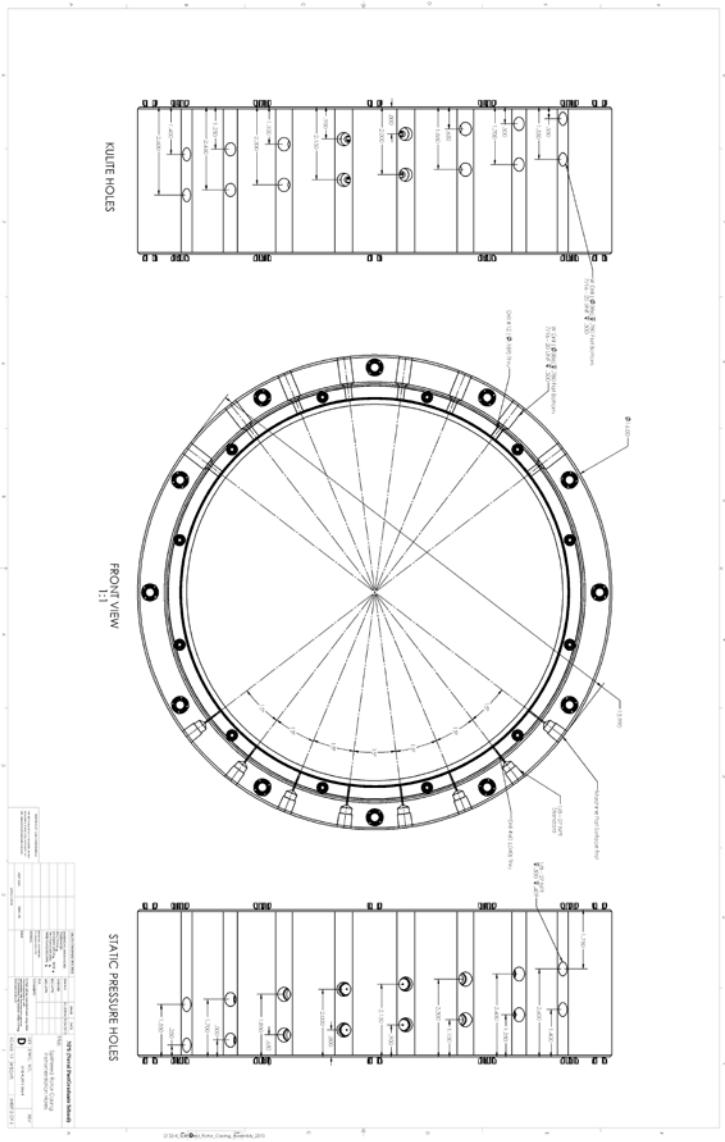
KULITE HOLES
FRONT VIEW
1:1
STATIC PRESSURE HOLES

FRONT VIEW
1 : 1
DETAIL G
8 : 1
SECTION F-F
1 : 1
Material: Suitable aluminum Alloy
Number:
D

APPENDIX E. STATOR DRAWINGS

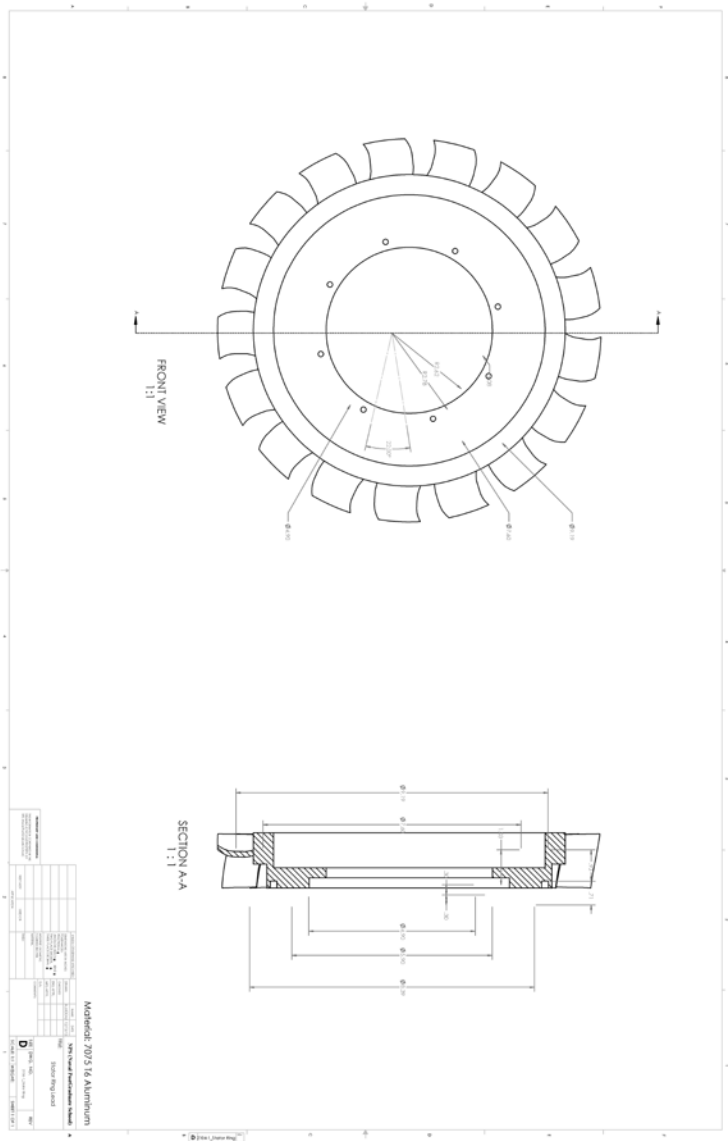

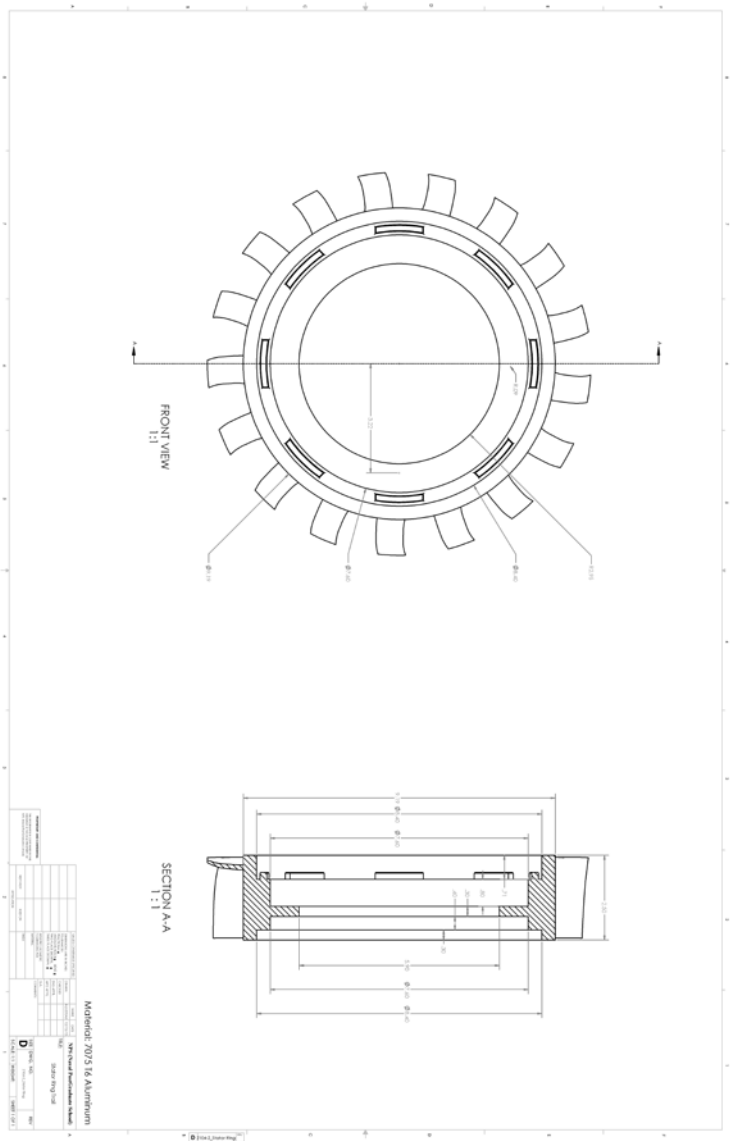
FRONT VIEW
1:1
SECTION A-A
1:1
Material: 7075 T6 Aluminum

LIST OF REFERENCES

[1] S. Drayton, "Design, test, and evaluation of a transonic axial compressor rotor with splitter blades," Ph.D. diss., Dept. Mech, and Aero. Eng., Naval Postgraduate School, Monterey, CA. Sept 2013.

[2] A. J. Wennerstrom, *Design of Highly Loaded Axial-Flow Fans and Compressors*, White River Junction, VT: Concepts ETI, Inc., 2000, p. 69.

[3] A. J. Wennerstrom, "Some experiments with a supersonic axial compressor stage," *ASME Journal of Turbomachiner*y, vol. 109, pp. 388–397, 1987.

[4] K. L. Tzuoo, S. S. Hingorani, and A.K. Sehra, "Design methodology for splittered axial compressor rotors," in *Gas Turbine and Aeroengine Congress and Exposition*, Brussels, Belgium, 1990.

[5] J. McClumphy, "Numerical investigation of subsonic axial-flow tandem airfoils for a core compressor rotor," Ph.D. diss., Dept. Mech. Eng., Virginia Polytechnic Institute and State University, Blacksburg, VA, 2008.

[6] M. H. Vavra, *Aero-Thermodynamics and Flow in Turbomachines*. Hoboken, NJ: J. Wiley & Sons, 1960.

[7] F. H. Breugelmans, Y. Y. Carels, and M. M. Demuth "Influence of Dihedral on the Secondary Flow in a Two-Dimensional Compressor Cascade." *J. Eng. Gas Turbines Power*, vol. 106, no. 3, pp. 578–584, 1984.

[8] T. Sasaki and F. A. E. Breugelmans, "Comparison of sweep and dihedral effects on compressor cascade performance." *ASME Journal of Turbomachinery*, vol. 120, no. 2, pp. 454-464, 1998.

[9] D. J. McNab, "Experimental testing and CFD modeling of an advanced transonic compressor for military applications," M.S. thesis, Dept. Mechanical and Aerospace Eng., Naval Postgraduate School, Monterey CA, 2011.

[10] A. Londoño, "Near-stall modal disturbances within a transonic compressor rotor," M.S. thesis, Dept. Mechanical and Aerospace Eng., Naval Postgraduate School, Monterey CA, 2011.

[11] B. L. Grossman, "Testing and analysis of a transonic axial compressor," M.S. thesis, Dept. Mechanical and Aerospace Eng., Naval Postgraduate School, Monterey CA, 1997.

[12] A. J. Gannon (private communication), 2013.

[13] G. Hobson et al., “Experimental and Numerical Performance Characterization of a Transonic Compressor Rotor Operating behind an Inlet-Guide Vane with Variable Flap Angles,” ASME TURBO EXPO paper GT2014-27308 to be presented in Dusseldorf, Germany, June 2014.

[14] S. Drayton, “TPL transonic axial compressor rotor design tool software,” Turbopropulsion Laboratory, Naval Postgraduate School, Monterey, CA, Tech. Note 13–01, Sep. 2013.

[15] F. M. White, *Fluid Mechanics*, 7th ed., New York: McGraw-Hill, 2011, p. 364.

INITIAL DISTRIBUTION LIST

1. Defense Technical Information Center
   Ft. Belvoir, Virginia

2. Dudley Knox Library
   Naval Postgraduate School
   Monterey, California